



Production of P-Wave Charm and Charm-Strange Mesons in Hadronic Z^0 Decays

The OPAL Collaboration

Abstract

Results are presented on the production of excited charm and excited charm-strange mesons in hadronic Z^0 decays. The results are obtained from approximately 4.3 million hadronic Z^0 decays, collected on or near the Z^0 resonance using the OPAL detector at LEP. The $D_1^0(2420)$ and $D_2^{*0}(2460)$ mesons are reconstructed in the $D^{*+}\pi^-$ final state and their separate production rates in charm fragmentation and in weak decays of b-hadrons are determined. From these measurements, the charm hadronization fractions and the inclusive branching ratios of b-hadrons to these neutral P-wave charm mesons are determined to be

$$\begin{aligned} f(c \rightarrow D_1^0) &= 0.021 \pm 0.007(\text{stat}) \pm 0.003(\text{syst}), \\ f(c \rightarrow D_2^{*0}) &= 0.052 \pm 0.022(\text{stat}) \pm 0.013(\text{syst}), \\ f(b \rightarrow D_1^0) &= 0.050 \pm 0.014(\text{stat}) \pm 0.006(\text{syst}), \\ f(b \rightarrow D_2^{*0}) &= 0.047 \pm 0.024(\text{stat}) \pm 0.013(\text{syst}). \end{aligned}$$

We also present the first observation at LEP of the $D_{s1}^+(2536)$ meson which is reconstructed in both the $D^{*+}K_S^0$ and $D^{*0}K^+$ final states. After correcting for the expected contribution from $b\bar{b}$ events, these results are used to derive the charm hadronization fraction $f(c \rightarrow D_{s1}^+)$:

$$f(c \rightarrow D_{s1}^+) = 0.016 \pm 0.004(\text{stat}) \pm 0.003(\text{syst}).$$

(To be submitted to Zeitschrift für Physik C)

The OPAL Collaboration

K. Ackerstaff⁸, G. Alexander²³, J. Allison¹⁶, N. Altekamp⁵, K.J. Anderson⁹, S. Anderson¹²,
S. Arcell², S. Asai²⁴, D. Axen²⁹, G. Azuelos^{18,a}, A.H. Ball¹⁷, E. Barberio⁸, R.J. Barlow¹⁶,
R. Bartoldus³, J.R. Batley⁵, S. Baumann³, J. Bechtluft¹⁴, C. Beeston¹⁶, T. Behnke⁸, A.N. Bell¹,
K.W. Bell²⁰, G. Bella²³, S. Bentvelsen⁸, P. Berlich¹⁰, S. Bethke¹⁴, O. Biebel¹⁴, A. Biguzzi⁵,
S.D. Bird¹⁶, V. Blobel²⁷, I.J. Bloodworth¹, J.E. Bloomer¹, M. Bobinski¹⁰, P. Bock¹¹,
D. Bonacorsi², M. Boutemeur³⁴, B.T. Bouwens¹², S. Braibant¹², L. Brigliadori², R.M. Brown²⁰,
H.J. Burckhart⁸, C. Burgard⁸, R. Bürgin¹⁰, P. Capiluppi², R.K. Carnegie⁶, A.A. Carter¹³,
J.R. Carter⁵, C.Y. Chang¹⁷, D.G. Charlton^{1,b}, D. Chrisman⁴, P.E.L. Clarke¹⁵, I. Cohen²³,
J.E. Conboy¹⁵, O.C. Cooke¹⁶, M. Cuffiani², S. Dado²², C. Dallapiccola¹⁷, G.M. Dallavalle², S. De
Jong¹², L.A. del Pozo⁴, K. Desch³, M.S. Dixit⁷, E. do Couto e Silva¹², M. Doucet¹⁸,
E. Duchovni²⁶, G. Duckeck³⁴, I.P. Duerdoth¹⁶, D. Eatough¹⁶, J.E.G. Edwards¹⁶,
P.G. Estabrooks⁶, H.G. Evans⁹, M. Evans¹³, F. Fabbri², M. Fanti², A.A. Faust³⁰, F. Fiedler²⁷,
M. Fierro², H.M. Fischer³, I. Fleck⁸, R. Folman²⁶, D.G. Fong¹⁷, M. Foucher¹⁷, A. Fürtjes⁸,
D.I. Futyan¹⁶, P. Gagnon⁷, J.W. Gary⁴, J. Gascon¹⁸, S.M. Gascon-Shotkin¹⁷, N.I. Geddes²⁰,
C. Geich-Gimbel³, T. Geralis²⁰, G. Giacomelli², P. Giacomelli⁴, R. Giacomelli², V. Gibson⁵,
W.R. Gibson¹³, D.M. Gingrich^{30,a}, D. Glenzinski⁹, J. Goldberg²², M.J. Goodrick⁵, W. Gorn⁴,
C. Grandi², E. Gross²⁶, J. Grunhaus²³, M. Gruwé⁸, C. Hajdu³², G.G. Hanson¹², M. Hansroul⁸,
M. Hapke¹³, C.K. Hargrove⁷, P.A. Hart⁹, C. Hartmann³, M. Hauschild⁸, C.M. Hawkes⁵,
R. Hawkings²⁷, R.J. Hemingway⁶, M. Herndon¹⁷, G. Herten¹⁰, R.D. Heuer⁸, M.D. Hildreth⁸,
J.C. Hill⁵, S.J. Hillier¹, T. Hilse¹⁰, P.R. Hobson²⁵, R.J. Homer¹, A.K. Honma^{28,a}, D. Horváth^{32,c},
R. Howard²⁹, D.E. Hutchcroft⁵, P. Igo-Kemenes¹¹, D.C. Imrie²⁵, M.R. Ingram¹⁶, K. Ishii²⁴,
A. Jawahery¹⁷, P.W. Jeffreys²⁰, H. Jeremie¹⁸, M. Jimack¹, A. Joly¹⁸, C.R. Jones⁵, G. Jones¹⁶,
M. Jones⁶, U. Jost¹¹, P. Jovanovic¹, T.R. Junk⁸, D. Karlen⁶, V. Kartvelishvili¹⁶, K. Kawagoe²⁴,
T. Kawamoto²⁴, R.K. Keeler²⁸, R.G. Kellogg¹⁷, B.W. Kennedy²⁰, J. Kirk²⁹, A. Klier²⁶,
S. Kluth⁸, T. Kobayashi²⁴, M. Kobel¹⁰, D.S. Koetke⁶, T.P. Kokott³, M. Kolrep¹⁰,
S. Komamiya²⁴, T. Kress¹¹, P. Krieger⁶, J. von Krogh¹¹, P. Kyberd¹³, G.D. Lafferty¹⁶,
R. Lahmann¹⁷, W.P. Lai¹⁹, D. Lanske¹⁴, J. Lauber¹⁵, S.R. Lautenschlager³¹, J.G. Layter⁴,
D. Lazic²², A.M. Lee³¹, E. Lefebvre¹⁸, D. Lellouch²⁶, J. Letts¹², L. Levinson²⁶, S.L. Lloyd¹³,
F.K. Loebinger¹⁶, G.D. Long²⁸, M.J. Losty⁷, J. Ludwig¹⁰, A. Macchiolo², A. Macpherson³⁰,
M. Mannelli⁸, S. Marcellini², C. Markus³, A.J. Martin¹³, J.P. Martin¹⁸, G. Martinez¹⁷,
T. Mashimo²⁴, P. Mättig³, W.J. McDonald³⁰, J. McKenna²⁹, E.A. Mckigney¹⁵, T.J. McMahon¹,
R.A. McPherson⁸, F. Meijers⁸, S. Menke³, F.S. Merritt⁹, H. Mes⁷, J. Meyer²⁷, A. Michelini²,
G. Mikenberg²⁶, D.J. Miller¹⁵, A. Mincer^{22,e}, R. Mir²⁶, W. Mohr¹⁰, A. Montanari², T. Mori²⁴,
M. Morii²⁴, U. Müller³, K. Nagai²⁶, I. Nakamura²⁴, H.A. Neal⁸, B. Nellen³, R. Nisius⁸,
S.W. O'Neale¹, F.G. Oakham⁷, F. Odorici², H.O. Ogren¹², N.J. Oldershaw¹⁶, M.J. Oreglia⁹,
S. Orito²⁴, J. Pálincás^{33,d}, G. Pásztor³², J.R. Pater¹⁶, G.N. Patrick²⁰, J. Patt¹⁰, M.J. Pearce¹,
S. Petzold²⁷, P. Pfeifenschneider¹⁴, J.E. Pilcher⁹, J. Pinfold³⁰, D.E. Plane⁸, P. Poffenberger²⁸,
B. Poli², A. Posthaus³, H. Przysiezniak³⁰, D.L. Rees¹, D. Rigby¹, S. Robertson²⁸, S.A. Robins²²,
N. Rodning³⁰, J.M. Roney²⁸, A. Rooke¹⁵, E. Ros⁸, A.M. Rossi², M. Rosvick²⁸, P. Routenburg³⁰,
Y. Rozen²², K. Runge¹⁰, O. Runolfsson⁸, U. Ruppel¹⁴, D.R. Rust¹², R. Rylko²⁵, K. Sachs¹⁰,
T. Saeki²⁴, E.K.G. Sarkisyan²³, C. Sbarra²⁹, A.D. Schaile³⁴, O. Schaile³⁴, F. Scharf³,
P. Scharff-Hansen⁸, P. Schenk³⁴, J. Schieck¹¹, P. Schleper¹¹, B. Schmitt⁸, S. Schmitt¹¹,

A. Schöning⁸, M. Schröder⁸, H.C. Schultz-Coulon¹⁰, M. Schulz⁸, M. Schumacher³, C. Schwick⁸, W.G. Scott²⁰, T.G. Shears¹⁶, B.C. Shen⁴, C.H. Shepherd-Themistocleous⁸, P. Sherwood¹⁵, G.P. Siroli², A. Sittler²⁷, A. Skillman¹⁵, A. Skuja¹⁷, A.M. Smith⁸, G.A. Snow¹⁷, R. Sobie²⁸, S. Söldner-Rembold¹⁰, R.W. Springer³⁰, M. Sproston²⁰, K. Stephens¹⁶, J. Steuerer²⁷, B. Stockhausen³, K. Stoll¹⁰, D. Strom¹⁹, P. Szymanski²⁰, R. Tafirot¹⁸, S.D. Talbot¹, S. Tanaka²⁴, P. Taras¹⁸, S. Tarem²², R. Teuscher⁸, M. Thiergen¹⁰, M.A. Thomson⁸, E. von Törne³, S. Towers⁶, I. Trigger¹⁸, E. Tsur²³, A.S. Turcot⁹, M.F. Turner-Watson⁸, P. Utzat¹¹, R. Van Kooten¹², M. Verzocchi¹⁰, P. Vikas¹⁸, E.H. Vokurka¹⁶, H. Voss³, F. Wäckerle¹⁰, A. Wagner²⁷, C.P. Ward⁵, D.R. Ward⁵, P.M. Watkins¹, A.T. Watson¹, N.K. Watson¹, P.S. Wells⁸, N. Wermes³, J.S. White²⁸, B. Wilkens¹⁰, G.W. Wilson²⁷, J.A. Wilson¹, G. Wolf²⁶, T.R. Wyatt¹⁶, S. Yamashita²⁴, G. Yekutieli²⁶, V. Zacek¹⁸, D. Zer-Zion⁸

¹School of Physics and Space Research, University of Birmingham, Birmingham B15 2TT, UK

²Dipartimento di Fisica dell' Università di Bologna and INFN, I-40126 Bologna, Italy

³Physikalisches Institut, Universität Bonn, D-53115 Bonn, Germany

⁴Department of Physics, University of California, Riverside CA 92521, USA

⁵Cavendish Laboratory, Cambridge CB3 0HE, UK

⁶Ottawa-Carleton Institute for Physics, Department of Physics, Carleton University, Ottawa, Ontario K1S 5B6, Canada

⁷Centre for Research in Particle Physics, Carleton University, Ottawa, Ontario K1S 5B6, Canada

⁸CERN, European Organisation for Particle Physics, CH-1211 Geneva 23, Switzerland

⁹Enrico Fermi Institute and Department of Physics, University of Chicago, Chicago IL 60637, USA

¹⁰Fakultät für Physik, Albert Ludwigs Universität, D-79104 Freiburg, Germany

¹¹Physikalisches Institut, Universität Heidelberg, D-69120 Heidelberg, Germany

¹²Indiana University, Department of Physics, Swain Hall West 117, Bloomington IN 47405, USA

¹³Queen Mary and Westfield College, University of London, London E1 4NS, UK

¹⁴Technische Hochschule Aachen, III Physikalisches Institut, Sommerfeldstrasse 26-28, D-52056 Aachen, Germany

¹⁵University College London, London WC1E 6BT, UK

¹⁶Department of Physics, Schuster Laboratory, The University, Manchester M13 9PL, UK

¹⁷Department of Physics, University of Maryland, College Park, MD 20742, USA

¹⁸Laboratoire de Physique Nucléaire, Université de Montréal, Montréal, Quebec H3C 3J7, Canada

¹⁹University of Oregon, Department of Physics, Eugene OR 97403, USA

²⁰Rutherford Appleton Laboratory, Chilton, Didcot, Oxfordshire OX11 0QX, UK

²²Department of Physics, Technion-Israel Institute of Technology, Haifa 32000, Israel

²³Department of Physics and Astronomy, Tel Aviv University, Tel Aviv 69978, Israel

²⁴International Centre for Elementary Particle Physics and Department of Physics, University of Tokyo, Tokyo 113, and Kobe University, Kobe 657, Japan

²⁵Brunel University, Uxbridge, Middlesex UB8 3PH, UK

²⁶Particle Physics Department, Weizmann Institute of Science, Rehovot 76100, Israel

²⁷Universität Hamburg/DESY, II Institut für Experimental Physik, Notkestrasse 85, D-22607 Hamburg, Germany

²⁸University of Victoria, Department of Physics, P O Box 3055, Victoria BC V8W 3P6, Canada

²⁹University of British Columbia, Department of Physics, Vancouver BC V6T 1Z1, Canada

³⁰University of Alberta, Department of Physics, Edmonton AB T6G 2J1, Canada

³¹Duke University, Dept of Physics, Durham, NC 27708-0305, USA

³²Research Institute for Particle and Nuclear Physics, H-1525 Budapest, P O Box 49, Hungary

³³Institute of Nuclear Research, H-4001 Debrecen, P O Box 51, Hungary

³⁴Ludwigs-Maximilians-Universität München, Sektion Physik, Am Coulombwall 1, D-85748 Garching, Germany

^a and at TRIUMF, Vancouver, Canada V6T 2A3

^b and Royal Society University Research Fellow

^c and Institute of Nuclear Research, Debrecen, Hungary

^d and Department of Experimental Physics, Lajos Kossuth University, Debrecen, Hungary

^e and Depart of Physics, New York University, NY 1003, USA

1 Introduction

In a $c\bar{q}$ meson system with $L = 0$, where L is the orbital angular momentum, for each light anti-quark flavour, \bar{q} , there are two possible meson spin states: spin-0 and spin-1. These correspond, respectively, to the pseudoscalar and vector $c\bar{q}$ ground state mesons. For $L = 1$, four $c\bar{q}$ meson states are predicted; a triplet of states and a singlet state coming, respectively, from the vector addition of one unit of orbital angular momentum to the spin-1 or spin-0 $c\bar{q}$ system. Heavy quark spin symmetry [1] suggests that the properties of these P-wave ($L = 1$) mesons are determined mainly by the total angular momentum of the light quark, $j_q = L + s_q$, where s_q represents the spin of the light quark. Thus, in the heavy-quark limit, the four states are grouped into two doublets according to whether $j_q = \frac{3}{2}$ or $\frac{1}{2}$.

Based on the measured masses of the states which have been experimentally observed, and on theoretical predictions for the masses of unobserved states, it is commonly assumed that the decays of the $L = 1$ excited charm and charm-strange mesons are dominated by two-body decays to $D^{(*)}\pi$ and $D^{(*)}K$, respectively. In this case, conservation of spin-parity dictates both the allowed decay channels for the individual states and the allowed partial waves [1, 2]. The members of the $j_q = \frac{1}{2}$ doublet decay through S-waves and are therefore expected to have widths of order 100 – 200 MeV/ c^2 . The states in the $j_q = \frac{3}{2}$ doublet, the $D_1^0(2420)$ and the $D_2^{*0}(2460)$, can decay only through D-waves. They are therefore rather narrow, with widths of order 20 MeV/ c^2 .

The six narrow states ($j_q = \frac{3}{2}$), corresponding to the three species of light anti-quark, have all been observed experimentally, by the ARGUS [3, 4, 5, 6] and CLEO [7, 8, 9] collaborations. Some of these states have also been observed at fixed target experiments[10, 11], in bubble chamber experiments [12] and at LEP[13, 14]. The properties of these states [15] are summarized in table 1. OPAL [16] and other LEP experiments [17, 18] have also provided evidence for P-wave B and B_s meson production in hadronic Z^0 decays.

In Z^0 decays, D^{**0} mesons¹ are produced both in charm fragmentation and as the decay products of b-flavoured hadrons. As these processes are physically distinct, it is desirable to determine these two contributions to the total D^{**0} production rate separately. Measurements of the production of these states in $Z^0 \rightarrow c\bar{c}$ events provides useful information about heavy-quark fragmentation since they are produced earlier in the fragmentation and decay chain than are the lighter D^* and D mesons. Also, the observation of both members of a $j_q = \frac{3}{2}$ doublet allows spin-counting assumptions about particle production to be tested. Similarly, measurement of $L = 1$ charm-strange meson production rates relative to their non-strange counterparts provides a test of assumptions about strange-quark suppression effects in the fragmentation process.

This paper describes measurements made with the OPAL detector at LEP. Section 2 provides a brief discussion of the detector as well as the data and Monte Carlo samples used. Section 3 describes measurements of the production rates for the $D_1^0(2420)$ and $D_2^{*0}(2460)$ mesons in charm and bottom enriched samples of hadronic Z^0 decays. These states are reconstructed

¹In this paper, the symbol D^{**0} represents an arbitrary mixture of the two states, $D_1^0(2420)$ and $D_2^{*0}(2460)$.

$L = 1$ State	Mass (MeV/ c^2)	Width Γ (MeV/ c^2)	Final States
D_1^0	2422.2 ± 1.8	$18.9^{+4.6}_{-3.5}$	$D^*\pi$
D_2^{*0}	2458.9 ± 2.0	23 ± 5	$D^*\pi, D\pi$
D_1^+	2427 ± 5	28 ± 8	$D^*\pi$
D_2^{*+}	2459 ± 4	25^{+8}_{-7}	$D^*\pi, D\pi$
D_{s1}^+	2535.35 ± 0.34	< 2.3 (90% CL)	D^*K
D_{s2}^{*+}	2573.5 ± 1.7	15^{+5}_{-4}	D^*K, DK

Table 1: Summary of the measured properties of the six narrow $L = 1$ charm mesons[15]. The last column shows the two-body final states allowed by spin-parity and isospin conservation.

through their decay² $D^{*0} \rightarrow D^{*+}(2010)\pi^-$. Section 4 presents a measurement of the D_{s1}^+ production rate in $Z^0 \rightarrow c\bar{c}$ events. This state is observed in both the $D^{*0}K^+$ and the $D^{*+}K_S^0$ final states. This measurement represents the first observation of this state at LEP.

2 The OPAL detector and data sample

A complete description of the OPAL detector can be found elsewhere [19]. However, aspects of the detector which are particularly pertinent to this analysis are briefly described here. The tracking of charged particles is performed by a large central jet chamber, a precision vertex drift chamber and chambers which measure the z -coordinate of tracks as they leave the jet chamber³. These detectors are located inside a uniform solenoidal field of 0.435 T. The jet chamber also provides measurements of the ionization energy loss (dE/dx) of charged particles. This information is used for charged-particle identification. In 1991, a high-precision silicon microvertex detector [20], providing two layers of silicon strip readout in the ϕ plane, was installed around a beryllium-composite beam pipe. This was upgraded in 1993 [21] with a new silicon detector which provides both ϕ and z information. For $Z^0 \rightarrow \mu^+\mu^-$ events, the detector achieves impact parameter resolutions of $15\mu\text{m}$ in $r - \phi$ and from $20 - 50\mu\text{m}$ in z , depending on the polar angle θ .

The solenoid coil is surrounded by an assembly of time-of-flight scintillators and an electromagnetic calorimeter consisting of lead-glass blocks instrumented with a presampler. These are located inside the iron return yoke of the magnet which is instrumented to serve as a hadronic calorimeter and is itself surrounded by several layers of muon chambers. A similar configuration of subdetectors is present in the end-cap regions of the detector.

This analysis makes use of approximately 4.3 million hadronic Z^0 decays recorded by OPAL in the region of the Z^0 resonance, between 1990 and 1995. The selection of hadronic Z^0 decays

²Charge conjugation is implied throughout this paper.

³The right-handed coordinate system used by OPAL has the z -axis along the electron beam and the y -axis pointing up. The polar angle θ and the azimuthal angle ϕ are defined with respect to the z - and x -axes, respectively.

used in this analysis has been described elsewhere [22]. For simulation studies, approximately 6 million five-flavour hadronic Monte Carlo events were generated, 2 million using JETSET 7.3 [23] and 4 million with JETSET 7.4 [24]. All Monte Carlo samples described in this paper were passed through a full simulation of the OPAL detector [25] and processed using the same reconstruction and selection algorithms used to process the raw data recorded with the detector. The D^0 and B meson lifetimes used were $\tau(D^0) = 0.415$ ps and $\tau(B) = 1.60$ ps, consistent with current world averages [15]. The fragmentation of heavy quarks was simulated using Peterson fragmentation parameters [26] tuned to reproduce measured values for the mean scaled energies of heavy mesons, $\langle x_E(B) \rangle = 0.695 \pm 0.010$ [27], $\langle x_E(D^+) \rangle = 0.483^{+0.007}_{-0.011}$ and $\langle x_E(D^0) \rangle = 0.487^{+0.017}_{-0.018}$ [28].

While JETSET can generate the full multiplet of heavy P-wave states, the wide $J^P = 1^+$ and 0^+ resonances were omitted. Since theoretical predictions for their natural widths are of order 100-200 MeV/ c^2 , these states are not expected to produce observable resonant structure in this analysis. The resonance parameters of the narrow P-wave charm mesons were set to values consistent with those compiled in 1996 by the Particle Data Group [15]. The ratio of the branching ratios for $D_{s2}^{*+}(2573)$ decays to D^*K and DK final states was set to 1/9, consistent with the CLEO limit [9]

$$\frac{\text{Br}(D_{s2}^{*+}(2573) \rightarrow D^*K)}{\text{Br}(D_{s2}^{*+}(2573) \rightarrow DK)} < 0.33 \quad \text{at 90\% C.L.} \quad (1)$$

and with theoretical predictions of 0.1 to 0.14 [29].

Two additional samples of $Z^0 \rightarrow c\bar{c}$ events containing D_{s1}^+ mesons were generated using JETSET 7.4. Approximately 8000 and 4000 events were generated with D_{s1}^+ mesons decaying to the $D^{*0}K^+$ and $D^{*+}K_S^0$ final states, respectively. These samples were used to study the mass resolution and efficiency for D_{s1}^+ reconstruction in each of these final states.

3 D_1^0 and D_2^{*0} production

In this analysis, the D_1^0 and D_2^{*0} states were reconstructed in the decay sequence

$$D^{**0} \longrightarrow D^*(2010)^+ \pi^- \begin{cases} \longleftarrow D^0 \pi^+ \\ \longleftarrow K^- \pi^+ \end{cases} \quad (2)$$

since the D^{*+} can be cleanly reconstructed through the decay chain $D^{*+} \rightarrow D^0 \pi^+$. The criteria for the selection of high-quality charged tracks and the D^{*+} reconstruction method were identical to those used previously by OPAL [30]. Only D^{*+} candidates having a scaled energy, $x_E(D^{*+}) \equiv E_{D^{*+}}/E_{\text{beam}}$, greater than 0.2 were accepted. Here, $E_{D^{*+}}$ and E_{beam} are the D^{*+} and beam energies, respectively. The invariant mass of each $K^- \pi^+$ combination was required to be within the range $1.79 < M(K^- \pi^+) < 1.94$ GeV/ c^2 and the mass-difference between the reconstructed

$D^0\pi^+$ combination and the D^0 was required to be in the range $142 < \Delta M(D^0\pi^+) < 149 \text{ MeV}/c^2$. The remaining D^{*+} selection criteria differed slightly for the accepted regions of $x_E(D^{*+})$ above and below 0.5, since the combinatorial background is largest at low energies. The pseudoscalar nature of the D^0 was used to reduce random $K^-\pi^+$ combinations by requiring that $|\cos\theta^*| < 0.8$ (0.9) when $x_E(D^{*+}) < (>)0.5$. Here, θ^* is the angle between the K^- and the D^0 boost direction, calculated in the D^0 rest frame. The K^- purity was enhanced by exploiting the particle identification capabilities of the OPAL jet chamber. Tracks were assigned dE/dx weights, w_x , according to the assumed particle species, x , the measured energy loss per unit length, and the corresponding uncertainty. These weights were signed according to whether the measured energy loss was greater or less than that expected for the assumed particle type. In the selection of D^{*+} candidates, the symmetric requirement $|w_K(K^-)| > 0.1$ was imposed on kaon track candidates for D^{*+} mesons with $x_E < 0.5$. No cut was applied for $x_E > 0.5$.

Finally, D^{**0} candidates were formed by selecting $D^{*+}\pi^-$ combinations, where the momentum of the pion candidate was required to exceed $2 \text{ GeV}/c$. This momentum cut was made in order to suppress pion candidates produced in quark fragmentation. These have a much softer momentum spectrum than the pions from D^{**0} decays.

The contributions to the inclusive D^{**0} rate were separated into the $b\bar{b}$ and $c\bar{c}$ components by using lifetime and energy information. In $Z^0 \rightarrow c\bar{c}$ events, D^{**0} mesons are produced near the beginning of the fragmentation chain and thus have a significantly harder x_E spectrum than those produced in the decays of b-flavoured hadrons. Furthermore, because of the longer b-hadron lifetime, D^0 mesons produced in b-hadron decays will decay, on average, further from the primary vertex than those produced in charm fragmentation. These differences were exploited to obtain D^{**0} samples which were enriched in each flavour. Each flavour-enriched sample, however, contained some residual contribution from the other. In order to properly account for this impurity, the rates in charm and bottom events were determined simultaneously.

In order to measure the individual production rates for the D_1^0 and D_2^{*0} , the D^{**0} signal must also be separated into contributions from these two states. This could be achieved simply by parameterizing the signal as the sum of two Breit-Wigners convoluted with the experimental mass resolution, with the mass and width of the D_1^0 and D_2^{*0} components fixed to their nominal values [15]. In this analysis, however, additional information from the angular distribution of the D^{**0} decay products is also used. The narrow $J^P = 1^+$ and 2^+ $L = 1$ states have distinct distributions of $\cos\alpha$, where α is defined as the angle between the π^- from the D^{**0} decay and the π^+ from the D^{*+} decay, in the rest frame of the D^{*+} . In the heavy-quark limit discussed earlier, these are of the form $1 + 3\cos^2\alpha$ for the D_1^0 and $\sin^2\alpha$ for the D_2^{*0} states, regardless of any spin alignment of the initial state [2].

Although the D_1^0 meson could be a mixture of $j_q = \frac{3}{2}$ (narrow) and $j_q = \frac{1}{2}$ (broad) states, it has been experimentally observed to decay with a $\cos\alpha$ distribution consistent with the form expected for an unmixed state [4, 8, 11]. Therefore, the angular distributions quoted above were included in a maximum likelihood fit in order to provide additional separation power between the two signal components and between signal and background, which is expected to have a $\cos\alpha$ distribution which is approximately isotropic.

The selection of the flavour-enriched samples is described below in sections 3.1 and 3.2. Section 3.3 describes the fit procedure used to simultaneously extract the D^{*0} rates in charm and bottom events. The treatment of systematic errors is described in section 3.4. The final results are presented in section 3.5 and are discussed further in section 3.6.

3.1 The c-enriched sample

The sample enriched in $Z^0 \rightarrow c\bar{c} \rightarrow D^{*0}X$ was obtained by requiring $x_E(D^{*0}) > 0.5$. Additional suppression of $b\bar{b}$ events was achieved by requiring $c\tau(D^0) < 0.03$ cm where $c\tau = M_{D^0}\ell_{xy}/p_{xy}$ is the apparent proper time of the D^0 decay, computed using M_{D^0} , the D^0 mass[15], its decay length ℓ_{xy} , and its momentum p_{xy} , measured in the plane transverse to the beam axis.

The reconstruction efficiency and purity of the selection were studied using Monte Carlo. After all selection criteria were applied, the efficiency was $(18.7 \pm 0.8)\%$ for D^{*0} mesons produced in charm fragmentation with $x_E > 0.5$. Accounting for the region of scaled energy below the cut, this corresponds to a selection efficiency for all $D^{*0} \rightarrow D^{*+}\pi^-$ decays in charm events of about 12%. Less than 2% of all such decays produced in b-events are accepted by these selection criteria. The charm-purity of the selected sample was 67%, with 20% of the $D^{*+}\pi^-$ candidates coming from $b\bar{b}$ events and the remainder from light-quark events.

Figure 1(a) shows the mass-difference distribution obtained using this selection. A clear enhancement is visible in the mass region of the excited charm states. The mass resolution is about $7 \text{ MeV}/c^2$, so this enhancement is rather broad relative to the width of a single D^{*0} state. This is due to overlapping contributions from the two narrow states. Figure 1(b) shows the effect of requiring that the helicity angle in the decay satisfies $|\cos \alpha| > 0.7$. As expected, based on the angular distributions discussed above, this suppresses both the background and the D_2^0 signal relative to the D_1^0 component.

The fit procedure and results, as well as the determination of the rate, corrected for the background from $b\bar{b}$ events, is described in section 3.3. This requires not only knowledge of the D^{*0} production rate in bottom events but also of the fraction of these in the D_1^0 state, since there is no reason to expect this fraction to be the same in charm and bottom events.

3.2 The b-enriched sample

A sample of $D^{*0} \rightarrow D^{*+}\pi^-$ decays produced mainly from decays of b-hadrons was obtained by reconstructing b-decay vertices in events containing D^{*+} candidates. Once a D^{*+} candidate was found, the b-vertex reconstruction algorithm assigned tracks to the primary Z^0 decay vertex, the candidate b-decay vertex, or to a subset of tracks unassociated with either vertex. Track assignment hypotheses were tested by fitting the primary vertex and the $B \rightarrow D^{*+}X$ vertex topology. This procedure includes a fit of the two-track D^0 vertex. The decay length of the D^0 candidate with respect to the b-decay vertex was included as a free parameter but its flight

vector was constrained by momentum conservation to point back to the b-vertex. Since the algorithm for the b-enrichment depends strongly on vertexing, this analysis was performed using only data taken while the silicon microvertex chamber was operational. This is true for approximately 86% of the OPAL hadronic data sample.

The algorithm first grouped tracks in the event into jets using a cone-based algorithm[31]. This jet-finding scheme defines the 4-momentum of a jet as the sum of the 4-momenta of the constituent tracks. Tracks within a cone of half-angle $R = 0.7$ radians were assigned to a single jet if the resulting jet energy, ε , exceeded 10 GeV.

An initial primary vertex for the event was determined using an iterative χ^2 minimization method which included the average LEP beamspot position, measured by OPAL[32], as a constraint. This initial primary vertex estimate used all high-quality tracks except those forming the D^{*+} candidate. Based on their contribution to the χ^2 of the fit, tracks inconsistent with the vertex position were removed. This procedure was repeated until all remaining tracks were consistent with the vertex position. An initial b-vertex was formed using a similar algorithm applied to those tracks in the D^{*+} jet which were not consistent with the primary vertex position. Tracks inconsistent with this b-vertex candidate were iteratively removed. This vertex fit was performed in two or three dimensions, depending on whether tracks had z -hits in the silicon detector.

The track assignments to the primary vertex and the b-vertex candidate were then optimized by fitting all vertices in which one track was moved from the primary vertex to the b-vertex, or *vice versa*. The track reassignment which gave the largest reduction in $\chi_{\text{total}}^2 = \chi_{\text{prim}}^2 + \chi_{\text{sec}}^2$ was retained and the procedure was iterated until no further re-assignment could reduce χ_{total}^2 . In $b\bar{b}$ events, typically about two tracks were reassigned by this procedure.

Finally, to improve the efficiency for assigning a D^{*0} decay pion to the b-vertex, tracks assigned to the primary vertex were reassigned to the b-vertex if this did not increase the χ_{total}^2 by more than 1.5. Thus, tracks produced with low transverse momentum with respect to the jet axis could be assigned to the b-vertex, even if they were also consistent with production at the primary vertex.

Displaced vertices were selected by requiring $S/\sigma_S > 2$ and $L/\sigma_L > -2$, where, S and L are the decay lengths of the b-vertex with respect to the primary and the D^0 vertex with respect to the b-vertex, respectively. The quantities σ_S and σ_L are the corresponding uncertainties. The S/σ_S and L/σ_L distributions for data and Monte Carlo are shown in figures 2 and 3 and indicate that the modelling of the vertex reconstruction in the Monte Carlo is adequate. These distributions are similar for the two and three-dimensional vertex reconstructions. Further comparisons of the agreement between data and Monte Carlo were made by examining the reconstructed b-vertex multiplicities and the relative frequency with which tracks identified as leptons were assigned to b-vertices. These comparisons provided qualitative checks that the b-decay multiplicity is modelled properly and that leptons from semileptonic b-decays are indeed preferentially assigned to the appropriate b-vertices. The agreement in both cases provided additional support for the adequacy of the Monte Carlo simulation. However, due to the different momentum spectra of leptons from semileptonic b decays and π^- mesons from $D^{*0} \rightarrow D^{*+}\pi^-$

decays, it was not possible to use this as an independent, quantitative determination of the D^{**0} reconstruction efficiency.

The D^{**0} candidates were reconstructed by combining the D^{*+} candidate with pion candidates selected from the tracks assigned to the corresponding b vertex. Backgrounds resulting from false secondary vertices reconstructed in charm or light-flavour events are small since these vertices are typically of lower multiplicity than those reconstructed in $b\bar{b}$ events.

The efficiency for reconstructing $D^{**0} \rightarrow D^{*+}\pi^-$ decays in $b\bar{b}$ events was $(6.3 \pm 0.8)\%$ for $x_E > 0.2$. In the Monte Carlo, about 15% of D^{**0} mesons produced in $b\bar{b}$ decays have $x_E < 0.2$. The efficiency for reconstructing a D^{**0} in a $b\bar{b}$ event, averaged over all x_E values, was therefore about 5.5%. The corresponding efficiency for selecting a D^{**0} from a $c\bar{c}$ event, with this selection, was about 0.7%. These efficiencies were obtained from Monte Carlo.

The mass-difference distribution of $D^{*+}\pi^-$ combinations in the b-enriched sample is shown in figure 4(a). Figure 4(b) shows the effect of imposing the requirement $|\cos \alpha| > 0.7$. The effect of this cut is consistent with that expected for the angular distributions described earlier. The fit procedure is described in the next section.

3.3 Fitting procedures

The rates of D^{**0} production in $b\bar{b}$ and $c\bar{c}$ events were determined by simultaneously fitting the distributions shown in figures 1(a) and 4(a). The rates were extracted from an unbinned likelihood fit in which both mass-difference and helicity angle information were used to discriminate between the two D^{**0} states and the background.

The likelihood functions used to fit the charm and bottom distributions were

$$\begin{aligned} \mathcal{L}_{c\bar{c}} = \prod_i & \left((f_c^{c\bar{c}} f_1^{c\bar{c}} + f_c^{b\bar{b}} f_1^{b\bar{b}}) s_1(x_i, \alpha_i) + (f_c^{c\bar{c}}(1 - f_1^{c\bar{c}}) + f_c^{b\bar{b}}(1 - f_1^{b\bar{b}})) s_2(x_i, \alpha_i) \right. \\ & \left. + (1 - f_c^{c\bar{c}} - f_c^{b\bar{b}}) b_c(x_i, \alpha_i) \right) \end{aligned} \quad (3)$$

$$\begin{aligned} \mathcal{L}_{b\bar{b}} = \prod_i & \left((f_b^{b\bar{b}} f_1^{b\bar{b}} + f_b^{c\bar{c}} f_1^{c\bar{c}}) s_1(x_i, \alpha_i) + (f_b^{b\bar{b}}(1 - f_1^{b\bar{b}}) + f_b^{c\bar{c}}(1 - f_1^{c\bar{c}})) s_2(x_i, \alpha_i) \right. \\ & \left. + (1 - f_b^{b\bar{b}} - f_b^{c\bar{c}}) b_b(x_i, \alpha_i) \right) \end{aligned} \quad (4)$$

where x_i and α_i represent the mass-difference and the helicity angle for the i^{th} $D^{*+}\pi^-$ combination, respectively. The functions $s_1(x_i, \alpha_i)$ and $s_2(x_i, \alpha_i)$ represent the mass-difference and helicity angle distributions of the D_1^0 and D_2^{*0} , respectively. They are the same in both likelihood functions. The functions $b_c(x_i, \alpha_i)$ and $b_b(x_i, \alpha_i)$ parameterize the background in the charm and b-enriched distributions, respectively. Each of the signal and background functions is the product of two functions, describing the mass-difference and helicity angle distributions respectively, *e.g.* $s_1(x_i, \alpha_i) = s_1^x(x_i) \cdot s_1^\alpha(\alpha_i)$. The mass-difference distributions for the signals consist of Breit-Wigner distributions convoluted with the mass resolution, σ_{x_i} (typically 7 MeV/ c^2), on an event-by-event basis. The resonance parameters for the D_1^0 and D_2^{*0} were

fixed to the world average values[15]. The mass-difference distribution for the background was parameterized by a function of the form $b_q^x(x) \propto e^{-B_q(x-m_\pi)}(x-m_\pi)^{C_q}$ where m_π is the π^\pm mass and B_q and C_q are free parameters, defined separately for the two flavours ($q = c, b$).

The signal and background functions for each mass-difference parameterization were multiplied by functions describing the corresponding helicity angle distribution:

$$\begin{aligned} s_1^\alpha(\alpha) &= 1 + 3 \cos^2 \alpha && D_1^0 \text{ state} \\ s_2^\alpha(\alpha) &= 1 - \cos^2 \alpha && D_2^{*0} \text{ state} \\ b_q^\alpha(\alpha) &= 1 + \beta_q \cos \alpha + \gamma_q \cos^2 \alpha && \text{background} \end{aligned} \quad (5)$$

where β_q and γ_q are parameters which describe the effective helicity structure of the background for each flavour-enriched sample, q .

In equation (3), the parameter $f_c^{c\bar{c}}$ is the fraction of $D^{*+}\pi^-$ candidates coming from D^{**0} production in $c\bar{c}$ events. The parameter $f_1^{c\bar{c}}$ specifies the fraction of this signal due to the D_1^0 state. Likewise, $f_b^{b\bar{b}}$ and $f_1^{b\bar{b}}$ in equation (4) are the D^{**0} signal fraction and the fraction of this signal due to the D_1^0 state, for $b\bar{b}$ events. The parameters $f_c^{b\bar{b}}$ and $f_b^{c\bar{c}}$ represent the fractions of the reconstructed D^{**0} signals in c and b -enriched samples coming from D^{**0} decays in $b\bar{b}$ and $c\bar{c}$ events, respectively, where

$$f_c^{b\bar{b}} = f_b^{b\bar{b}} \frac{N_b \varepsilon_c^{b\bar{b}}}{N_c \varepsilon_b^{b\bar{b}}}, \quad (6)$$

and similarly for $f_b^{c\bar{c}}$. Here, N_b and N_c are the numbers of $D^{*+}\pi^-$ combinations accepted in each flavour-enriched sample and $\varepsilon_b^{b\bar{b}}$ and $\varepsilon_c^{b\bar{b}}$ are the efficiencies for accepting a D^{**0} from a $b\bar{b}$ event in the bottom and charm-enriched selections, respectively, corrected for unmeasured x_E regions. Since D^{**0} production in charm events is observed only for $x_E > 0.5$, it is necessary to perform such a correction to estimate the expected background in the b -enriched sample. Both the efficiencies and the corrections were obtained from Monte Carlo.

The fit was performed with 12 freely varying parameters: $f_c^{c\bar{c}}$, $f_1^{c\bar{c}}$, $f_b^{b\bar{b}}$ and $f_1^{b\bar{b}}$, which specified the D^{**0} production rates and D_1^0 signal fractions in $c\bar{c}$ and $b\bar{b}$ events, and B_q , C_q , β_q and γ_q , specified separately for $q = c, b$, which defined the shapes and helicity structures of the backgrounds in the two flavour-enriched samples.

The results of the fits to the charm and bottom-enriched mass-difference distributions, shown in figures 1(a) and 4(a), yield D^{**0} signals of 147 ± 37 events and 106 ± 24 events, respectively. Figures 1(b) and 4(b) show the mass-difference distributions obtained with the requirement that $|\cos \alpha| > 0.7$. The fit results shown in these figures are not independent of those shown in figures 1(a) and 4(a), but were obtained from the fit to the full distribution by integrating it over this range of $\cos \alpha$. The background and the D_2^{*0} signal are suppressed with respect to the D_1^0 signal. This behaviour is expected from the helicity angle distributions assumed for the D_1^0 , D_2^{*0} and background components in the fit. The level of the background for $|\cos \alpha| > 0.7$ is also seen to be described well in both the $b\bar{b}$ and $c\bar{c}$ distributions.

The mean multiplicity of $D^{**0} \rightarrow D^{*+}\pi^-$ decays produced in $Z^0 \rightarrow c\bar{c}$ events, for $x_E(D^{**0}) >$

0.5, is obtained from $f_c^{c\bar{c}}$ using

$$\bar{n}_{Z^0 \rightarrow c\bar{c} \rightarrow D^{*0}(x_E > 0.5)} \cdot \text{Br}(D^{*0} \rightarrow D^{*+}\pi^-) = \frac{N_{c\bar{c}} f_c^{c\bar{c}}}{N_{\text{MH}} \varepsilon'_{cc}} \cdot \frac{1}{\text{Br}(D^{*+} \rightarrow D^0\pi^+) \text{Br}(D^0 \rightarrow K^-\pi^+)}. \quad (7)$$

Here, N_{MH} is the number of hadronic events analysed and ε'_{cc} is the efficiency for reconstructing the D^{*0} decay, determined only for the accepted region of scaled energy, $x_E > 0.5$. A similar expression relates the fraction $f_b^{b\bar{b}}$ to the mean multiplicity of $D^{*0} \rightarrow D^{*+}\pi^-$ decays with $x_E > 0.2$ in $b\bar{b}$ events. The efficiencies are taken from Monte Carlo studies.

Correcting for the efficiencies and branching ratios, which were taken to be $\text{Br}(D^{*+} \rightarrow D^0\pi^+) \cdot \text{Br}(D^0 \rightarrow K^-\pi^+) = (2.616 \pm 0.089)\%$ [15], yields the following measurements of the mean multiplicity for D^{*0} production in $Z^0 \rightarrow c\bar{c}$ and $Z^0 \rightarrow b\bar{b}$ events:

$$\bar{r}_{c\bar{c}} \equiv \bar{n}_{Z^0 \rightarrow c\bar{c} \rightarrow D^{*0}(x_E > 0.5)} \cdot \text{Br}(D^{*0} \rightarrow D^{*+}\pi^-) = (5.4^{+1.4}_{-1.3}) \times 10^{-3} \quad (8)$$

$$\bar{r}_{b\bar{b}} \equiv \bar{n}_{Z^0 \rightarrow b\bar{b} \rightarrow D^{*0}(x_E > 0.2)} \cdot \text{Br}(D^{*0} \rightarrow D^{*+}\pi^-) = (16.1^{+3.7}_{-3.6}) \times 10^{-3}. \quad (9)$$

The fractions of these signals due to the D_1^0 state, in $c\bar{c}$ and $b\bar{b}$ events were

$$f_1^{c\bar{c}} = 0.56 \pm 0.15 \quad (10)$$

and

$$f_1^{b\bar{b}} = 0.77^{+0.16}_{-0.14}. \quad (11)$$

The quoted errors are statistical only. The correlation coefficient between the measured rates, $\bar{r}_{b\bar{b}}$ and $\bar{r}_{c\bar{c}}$, was -0.308 . The correlation coefficients between $\bar{r}_{c\bar{c}}$ and $f_1^{c\bar{c}}$ and between $\bar{r}_{b\bar{b}}$ and $f_1^{b\bar{b}}$ were -0.089 and -0.419 , respectively. These correlations are accounted for in section 5 where these numbers are used to derive other results.

3.4 Treatment of systematic errors

Contributions to the systematic uncertainties in the measured rates have been investigated in detail. The dominant sources are from uncertainties in the reconstruction efficiency, other aspects of Monte Carlo modelling, and inputs to the fit. All contributions are discussed below and summarized in table 2.

The contribution to the systematic error coming from uncertainties on the measured D_1^0 and D_2^{*0} resonance parameters was estimated by varying them within their one standard deviation errors. The changes in the measured quantities resulting when each resonance parameter was varied individually were added in quadrature. Also, the mass-difference resolution was scaled by factors ranging between 0.75 to 1.25 to estimate the effect of imperfect determination of the track parameter error matrices.

The D^{*0} production rates in $c\bar{c}$ and $b\bar{b}$ events were determined for different ranges of scaled energy. Calculating the efficiencies with which opposite-flavour decays populate the flavour-enriched mass-difference distributions required extrapolation into unmeasured x_E regions. The

D^{**0} rate in $c\bar{c}$ events was determined only for $x_E > 0.5$, but this rate was extrapolated to lower values of scaled energy in order to estimate the fraction of the D^{**0} signal in the b-enriched sample that was actually due to charm events. Likewise, the fraction of the D^{**0} signal in $b\bar{b}$ events having $x_E > 0.5$ was used to estimate the signal fraction in the c-enriched sample which was actually due to bottom events. Both of these extrapolations were performed using the Monte Carlo. This introduces a dependence on the fragmentation parameters used. The central values used for the Peterson fragmentation parameters [26] were $\epsilon_c = 0.031$ and $\epsilon_b = 0.0038$, tuned to reproduce the mean scaled energy of B and D hadrons [27, 28]. The uncertainties in these measurements (see section 2) motivated variation of these parameters over the ranges $0.018 < \epsilon_c < 0.044$ and $0.0018 < \epsilon_b < 0.0068$. The corresponding variations in the final result were used to estimate the size of the associated systematic effects.

Systematic uncertainties due to the lifetimes of B^0 and B^+ mesons used in the Monte Carlo were studied by reweighting the reconstruction efficiencies with these lifetimes varied by $\pm 5\%$, a range similar to the precision of current world averages[15]. The D^0 lifetime has been measured to within 1%. Variation of its lifetime within this uncertainty had a negligible effect on the final result. Effects due to imperfect tracking resolution, which could influence the vertex reconstruction and flavour separation, were estimated with Monte Carlo by redetermining the efficiencies with the resolutions of the track angles and impact parameters changed by $\pm 10\%$.

The minimum momentum requirement applied to the π^- from the D^{**0} decay limits the acceptance to decays in which the π^- is emitted preferentially in the forward direction. In the case of the charm-enriched sample, the minimum momentum cut corresponds approximately to a requirement of $\cos\theta_\pi > -0.6$. For the b-enriched sample, the acceptance is approximately limited to $\cos\theta_\pi > -0.3$. Here, θ_π is the decay angle of the π^- in the rest frame of the D^{**0} .

The limited $\cos\theta_\pi$ acceptance introduces two sources of systematic uncertainty since spin-alignment effects can produce a non-uniform distribution in $\cos\theta_\pi$. This non-uniformity takes different forms depending on the D^{**0} spin-alignment, but can be parameterized in terms of even powers of $\cos\theta_\pi$, since odd powers are forbidden by parity conservation. The Monte Carlo samples were generated with an isotropic distribution, so the efficiencies might require reweighting to correct for the unmeasured region. To investigate this effect, the $\cos\theta_\pi$ distribution was obtained by determining the D^{**0} rate in bins of $\cos\theta_\pi$. This distribution was fitted with the function $1 + a \cos^2\theta_\pi$ where a was determined to be 0.0 ± 1.0 for the charm-enriched and 0.8 ± 1.1 for the bottom-enriched samples. These values are consistent with zero, providing no evidence for non-isotropic distributions in $\cos\theta_\pi$. Nevertheless, variation of these parameters by their fitted uncertainties was used to assign a systematic error to account for possible non-uniform distributions arising from D^{**0} spin-alignment. Due to limited statistics, decay angle distributions with fourth powers of $\cos\theta_\pi$ were not considered. Although such contributions are allowed for individual helicity states of D_2^{*0} mesons, a mixture of several states reduces this effect. Thus, the polynomial form of $\cos\theta_\pi$ studied was considered adequate for the purpose of estimating systematic uncertainties.

The second source of uncertainty introduced by the limited $\cos\theta_\pi$ acceptance arises due to the fact that a restricted range of $\cos\theta_\pi$ can modify the expected $\cos\alpha$ distribution of D_1^0 decays, as discussed in [8]. The systematic error associated with this effect was estimated by

Source	$\Delta\bar{r}_{c\bar{c}} \times 10^{-3}$	$\Delta\bar{r}_{b\bar{b}} \times 10^{-3}$	$\Delta f_1^{c\bar{c}}$	$\Delta f_1^{b\bar{b}}$
Resonance parameters	+0.21 -0.21	+1.0 -0.9	+0.023 -0.022	+0.038 -0.040
Resolution scale	+0.15 -0.23	+0.6 -0.6	+0.021 -0.024	+0.007 -0.000
Fragmentation parameters	+0.15 -0.08	+0.1 -0.0	+0.006 -0.004	+0.000 -0.001
B lifetime	+0.03 -0.00	+0.3 -0.3	+0.001 -0.001	+0.000 -0.000
Track resolution	+0.04 -0.00	+0.9 -0.6	+0.004 -0.004	+0.001 -0.005
$\cos\theta_\pi$ acceptance (efficiency)	+0.34 -0.65	+0.6 -0.7	+0.004 -0.006	+0.001 -0.001
$\cos\theta_\pi$ acceptance (D_1^0 spin-alignment)	+0.06 -0.23	+0.3 -0.2	+0.008 -0.014	+0.009 -0.004
D_1^0 helicity ($1+B\cos^2\alpha$)	+0.03 -0.15	+0.1 -0.1	+0.000 -0.005	+0.012 -0.010
Monte Carlo statistics	+0.23 -0.23	+1.0 -1.0	—	—
$\text{Br}(D^{*+} \rightarrow D^0\pi^+) \cdot \text{Br}(D^0 \rightarrow K^-\pi^+)$	+0.20 -0.20	+0.6 -0.6	—	—
Total	+0.55 -0.82	+2.0 -1.8	+0.033 -0.036	+0.039 -0.041

Table 2: Summary of systematic uncertainties for the D^{*0} production rates and D_1^0 signal fractions. The rates $\bar{r}_{c\bar{c}}$ and $\bar{r}_{b\bar{b}}$ are defined in equations (8) and (9) respectively.

calculating the $\cos\alpha$ distribution for a limited $\cos\theta_\pi$ acceptance, as a function of the D_1^0 spin-alignment. Because of parity invariance, this can be specified in terms of a single spin density matrix element, which was varied between 0 and 1.

The systematic uncertainty associated with the assumption of a $1 + 3\cos^2\alpha$ form for the D_1^0 helicity angle distribution was estimated by refitting using the function $1 + B\cos^2\alpha$ where the value of B was varied between 1.81 and 4.14. This range corresponds to the uncertainty on a CLEO[8] measurement of B , derived from a fit to the D_1^0 helicity angle distribution.

Finally, contributions to the systematic error were assigned for uncertainties related to limited Monte Carlo statistics and imperfect knowledge of the $D^{*+} \rightarrow D^0\pi^+$ and $D^0 \rightarrow K^-\pi^+$ branching ratios.

As a cross-check, the selection criteria most sensitive to Monte Carlo modelling were varied to assess the stability of these results. The following modifications were made to the selection:

- The minimum momentum cut imposed on the π^- was varied from 1.5 to 2.5 GeV/ c .
- The maximum proper time ($c\tau$) for D^0 decays in the charm sample was varied from 0.01 to 0.05 cm.
- The S/σ_S cut was varied between 0 and 4 standard deviations.
- The L/σ_L cut was varied between -4 and 0 standard deviations.

In all cases, the variations in the D^{*0} production rates and D_1^0 signal fractions were consistent with being statistical in nature. Since there was no evidence for systematic effects not already accounted for, no additional systematic errors were assigned.

Finally, because the charm and bottom enhanced samples are not mutually exclusive, a study was performed to determine the fraction of the signals common to both selections. This study indicated that 11 ± 4 $D^{**0} \rightarrow D^{*+}\pi^-$ decays were common to the two samples. This is consistent with the number expected from the the measured rates and the Monte Carlo efficiencies for decays passing both selections.

3.5 Results

Accounting for the systematic errors discussed in the previous section, the results presented at the end of section 3.3 become:

$$\bar{n}_{Z^0 \rightarrow c\bar{c} \rightarrow D^{**0}(x_E > 0.5)} \cdot \text{Br}(D^{**0} \rightarrow D^{*+}\pi^-) = \left(5.4^{+1.4}_{-1.3} {}^{+0.6}_{-0.8}\right) \times 10^{-3} \quad (12)$$

$$\bar{n}_{Z^0 \rightarrow b\bar{b} \rightarrow D^{**0}(x_E > 0.2)} \cdot \text{Br}(D^{**0} \rightarrow D^{*+}\pi^-) = \left(16.1^{+3.7}_{-3.6} {}^{+2.0}_{-1.8}\right) \times 10^{-3} \quad (13)$$

and

$$f_1^{c\bar{c}} = 0.56 \pm 0.15 {}^{+0.03}_{-0.04} \quad (14)$$

$$f_1^{b\bar{b}} = 0.77 {}^{+0.16}_{-0.14} \pm 0.04. \quad (15)$$

where the errors are statistical and systematic, respectively.

3.6 Calculation of $f(c \rightarrow D^{**0})$ and $f(b \rightarrow D^{**0})$

The rates expressed in equations (12) and (13) were extrapolated to the full range of x_E using factors determined from the Monte Carlo. The fragmentation parameters used were tuned to reproduce the mean x_E values of B^{+0} and D^{+0} mesons, as described in section 3.4. Assuming quark fragmentation to D^{**0} and b-hadron states to be independent of x_E , this yields

$$2 \cdot \frac{\Gamma_{c\bar{c}}}{\Gamma_{\text{had}}} \cdot f(c \rightarrow D^{**0}) \cdot \text{Br}(D^{**0} \rightarrow D^{*+}\pi^-) = \left(8.4^{+2.2}_{-2.1} {}^{+0.9}_{-1.3} {}^{+0.4}_{-0.5}\right) \times 10^{-3} \quad (16)$$

$$2 \cdot \frac{\Gamma_{b\bar{b}}}{\Gamma_{\text{had}}} \cdot f(b \rightarrow D^{**0}) \cdot \text{Br}(D^{**0} \rightarrow D^{*+}\pi^-) = \left(18.3^{+4.2}_{-4.1} {}^{+2.3}_{-2.1} {}^{+0.4}_{-0.5}\right) \times 10^{-3}. \quad (17)$$

Here, $f(c \rightarrow D^{**0})$ is the fraction of charm quarks producing a D^{**0} in fragmentation and $f(b \rightarrow D^{**0})$ is the inclusive branching fraction, at the Z^0 , of b-hadrons into $D^{**0}X$. The second systematic error indicates the uncertainty on the extrapolation, including a contribution from the use of different fragmentation models[33]. In each case the fragmentation model parameters used were those obtained from fits to OPAL results on the production of weakly-decaying bottom and charm hadrons in hadronic Z^0 decays[27, 28].

The fraction of charm quarks which fragment to form either a D_1^0 or a D_2^{*0} was determined using the values from equations (14) and (16). The value of $\text{Br}(D_1^0 \rightarrow D^{*+}\pi^-)$ is constrained to be 0.65 by phase-space and isospin symmetry. Isospin considerations along with measurements of $\text{Br}(D_2^{*0} \rightarrow D^+\pi^-)/\text{Br}(D_2^{*0} \rightarrow D^{*+}\pi^-) = (2.3 \pm 0.6)$ [15] yield $\text{Br}(D_2^{*0} \rightarrow D^{*+}\pi^-) = (0.21 \pm 0.04)$.

Using these values, we estimate the charm hadronization factors, $f(c \rightarrow D_1^0)$ and $f(c \rightarrow D_2^{*0})$, defined as the fractions of charm quarks producing these states in fragmentation. This yields

$$f(c \rightarrow D_1^0) = 0.021 \pm 0.007 \pm 0.003 \quad (18)$$

$$f(c \rightarrow D_2^{*0}) = 0.052 \pm 0.022 \pm 0.013, \quad (19)$$

where the standard model expectation[34] $\Gamma_{c\bar{c}}/\Gamma_{\text{had}} = 0.172$ has been used. Hence, the fraction of charm quarks producing neutral narrow P-wave charm mesons is determined to be

$$f(c \rightarrow D^{**0}) = 0.073 \pm 0.023 \pm 0.014 \quad (20)$$

where the appropriate correlations have been accounted for. The corresponding fractions can also be calculated for the production of these states in b events using the standard model value of $\Gamma_{b\bar{b}}/\Gamma_{\text{had}} = 0.216$ [34]:

$$f(b \rightarrow D_1^0) = 0.050 \pm 0.014 \pm 0.006 \quad (21)$$

$$f(b \rightarrow D_2^{*0}) = 0.047 \pm 0.024 \pm 0.013. \quad (22)$$

From these values we obtain the inclusive branching ratio of b-hadrons to D^{**0} mesons:

$$f(b \rightarrow D^{**0}) = 0.097 \pm 0.035 \pm 0.017. \quad (23)$$

These results are discussed further in section 5.

4 $D_{s1}^+(2536)$ production in charm fragmentation

The D_{s1}^+ corresponds to the $J^P = 1^+$ state of the $j_q = \frac{3}{2}$ doublet of $c\bar{s}$ mesons discussed in the introduction. As such, the only allowed final states for its decay are $D^{*+}K^0$ and $D^{*0}K^+$. The very narrow width of this state ($\Gamma < 2.3 \text{ MeV}/c^2$ at 90% CL[15]) is attributed to its proximity to threshold for both of these final states. The narrow width of this state makes it easier to observe than its $J^P = 2^+$ partner. That state, the $D_{s2}^{*+}(2573)$, has a natural width of $15_{-4}^{+5} \text{ MeV}/c^2$ and lies well above the threshold of both final states that are available.

The D_{s1}^+ can be reconstructed in both final states. Reconstruction of the $D^{*0}K^+$ final state involves either the reconstruction of the π^0 or γ from the D^{*0} decay or the use of a partial reconstruction which does not require detection of the neutral particle. The analysis presented here uses a partial reconstruction technique introduced by the ARGUS collaboration [6].

Reconstruction of the D_{s1}^+ in the $D^{*+}K_S^0$ decay mode provides the best signal to background ratio since it can exploit the clean, well-understood signals obtainable for the D^{*+} and K_S^0 mesons. However, for the single D^0 decay channel used in this analysis, this reconstruction suffers from a small product of efficiency and branching ratios. With the available statistics, this means that the expected signal in this channel is quite small, relative to that obtainable in the $D^{*0}K^+$ final state.

While isospin invariance requires that the matrix elements for decays to the two final states be the same, the larger Q -value for the $D^{*0}K^+$ final state, relative to $D^{*+}K^0$, results in a 12% increase in the momentum of the final state particles, in the D_{s1}^+ rest frame. This can result in up to a 75% kinematic enhancement of the branching ratio to the $D^{*0}K^+$ final state, relative to $D^{*+}K^0$. This number comes from the expectation that the relative enhancement is given by

$$R \equiv \frac{\text{Br}(D_{s1}^+ \rightarrow D^{*0}K^+)}{\text{Br}(D_{s1}^+ \rightarrow D^{*+}K^0)} = \left(\frac{q_{D^{*0}K^+}}{q_{D^{*+}K^0}} \right)^{2L+1} \approx 1.75 \quad (24)$$

where q represents the momentum of the final state particles in the D_{s1}^+ rest frame. The factor of 1.75 comes from the assumption of a pure D-wave decay, *i.e.* $L=2$ in the above expression. CLEO has measured $R=1.1 \pm 0.3$ [7] while the ratio of the two ARGUS results[5, 6] yields $R=1.4 \pm 0.6$.

In this analysis, both final states were reconstructed. Section 4.1 describes the analysis of the $D^{*0}K^+$ final state. Section 4.2 describes D_{s1}^+ reconstruction in the $D^{*+}K_s^0$ final state. A calculation of the total rate for D_{s1}^+ production in $Z^0 \rightarrow c\bar{c}$ events is presented in section 4.3.

4.1 Analysis of the $D^{*0}K^+$ final state

The analysis of this final state utilized a partial reconstruction of the decay sequence

$$\begin{array}{ccc} D_{s1}^+(2536) & \longrightarrow & D^{*0}K^+ \\ & & \swarrow \\ & & D^0(\pi^0, \gamma) \\ & & \searrow \\ & & K^-\pi^+ \end{array} \quad (25)$$

in which the π^0 or γ from the D^{*0} decay was not identified. The low Q -value for the D^{*0} decay means that non-observation of the neutral particle does not greatly affect the mass reconstruction. A peak arising from this decay sequence should be observable in the invariant mass distribution of D^0K^+ combinations. The presence of an unobserved neutral particle simply shifts the peak to a lower mass and slightly degrades the mass resolution. Instead of looking at a D^0K^+ invariant mass distribution, we examined the mass-difference distribution

$$\Delta M(D^0K^+) \equiv M(D^0K^+) - M(D^0) \quad (26)$$

in which a peak arising from the decay sequence (25) should have a central value which does not depend on whether the neutral particle has been reconstructed. Use of the mass-difference technique also results in a better signal resolution than can be achieved using the invariant mass distribution.

The $D^0 \rightarrow K^-\pi^+$ candidates were selected from oppositely charged pairs of tracks, each with momentum greater than 6 GeV/ c . The invariant mass of each combination was required to be within the range $1.79 < M(K^-\pi^+) < 1.94$ GeV/ c^2 and the scaled energy, $x_E \equiv E_{D^0}/E_{\text{beam}}$, was required to exceed 0.45. In order to suppress combinatorial background, we required

$|\cos \theta^*| < 0.9$. Here, θ^* is the D^0 decay angle, defined as the angle between the kaon and the D^0 boost vector in its rest frame. Additional suppression of combinatorial background due to particles produced at the primary vertex was achieved using lifetime information. The decay length of the reconstructed $K^-\pi^+$ vertex was required to be displaced with respect to the primary vertex by at least 0.5 standard deviations. D^0 mesons from $D^{*+} \rightarrow D^0\pi^+$ decays were suppressed by rejecting D^0 candidates if combination with any π^+ candidate in the event yielded a mass-difference, $\Delta M(D^0\pi^+) = M(D^0\pi^+) - M(D^0)$, which was less than $0.16 \text{ GeV}/c^2$.

The dE/dx information from the OPAL jet chamber was used to enhance the purity of the kaon sample. Kaon candidates were rejected if their measured energy loss yielded a signed weight in the range $-0.05 < w_K(K) < 0.15$. This asymmetric window preferentially rejects pions since these deposit more dE/dx than do kaons of the same momentum, above $600 \text{ MeV}/c$. Pion candidates were required to satisfy $|w_\pi(\pi)| > 0.01$. Finally, to reject $\bar{D}^0 \rightarrow K^+\pi^-$ decays where the π^- and K^+ were incorrectly identified as K^- and π^+ , the weights were required to satisfy $|w_K(K^-)w_\pi(\pi^+)| > |w_\pi(K^-)w_K(\pi^+)|$.

To partially reconstruct $D_{s1}^+ \rightarrow D^{*0}K^+$ decays, D^0 candidates were combined with positively charged kaon candidates. The kaons were required to satisfy $-0.05 < w_K(K) < 0.15$ and to have momenta greater than $5.5 \text{ GeV}/c$. Combined with the x_E requirement on the D^0 candidate, this imposed an effective cut on the scaled energy of the D^0K^+ of $x_E > 0.57$. Because of the missing neutral particle in the D^{*0} decay, this corresponds closely to selecting D_{s1}^+ decays with $x_E > 0.6$. The Monte Carlo simulation yields an efficiency of $(9.0 \pm 0.7)\%$ for selecting $D_{s1}^+ \rightarrow D^{*0}K^+$ decays with $x_E > 0.6$.

This selection was applied to 6 million hadronic Monte Carlo events. The resulting mass-difference distribution is shown in figure 5(a). The hatched peak near threshold indicates the contribution from true $D_{s1}^+ \rightarrow D^{*0}K^+$ decays. Before detector resolution effects are considered, the D^0K^+ mass-difference resulting from a $D_{s1}^+ \rightarrow D^{*0}K^+$ decay depends on the angle at which the unobserved π^0 or γ is emitted, in the rest frame of the D^{*0} . An approximately uniform distribution of this decay angle leads to D^0K^+ mass differences uniformly distributed between the allowed kinematic limits. Thus, the form of the D_{s1}^+ signal in this channel consisted of two uniform distributions, weighted by the $D^{*0} \rightarrow D^0\pi^0$ and $D^{*0} \rightarrow D^0\gamma$ branching ratios, and convoluted with the expected detector resolution, determined from Monte Carlo studies. The curve overlaid on figure 5(a) is the result of an unbinned likelihood fit in which the signal was parameterized in this way. In this fit, the background shape was described by the functional form $b(x) \propto e^{-B(x-m_K)}(x-m_K)^C$, where m_K is the charged kaon mass and B and C are free parameters.

The fitted number of D_{s1}^+ decays reconstructed in the Monte Carlo was 28.5 ± 8.1 , consistent with the 27 events which were actually present. Although the width of the signal was fixed by the kinematics and detector resolution, its position was freely varied. The fitted mass-difference was $525.7 \pm 2.1 \text{ MeV}/c^2$, consistent with the generated value of $528.3 \text{ MeV}/c^2$. Allowing the width to vary yielded a Gaussian width of $6.0 \pm 2.2 \text{ MeV}/c^2$, consistent with the expectation of $7 \pm 1 \text{ MeV}/c^2$ derived from the high statistics $D_{s1}^+ \rightarrow D^{*0}K^+$ Monte Carlo sample.

Figure 5(a) also shows the entries from direct $D_{s2}^{*+} \rightarrow D^0K^+$ decays. Since the partial

Source	Uncertainty $\times 10^{-3}$
Background parameterization	+0.10 -0.04
Signal parameterization	+0.09 -0.12
Tracking resolution	+0.04 -0.04
dE/dx modelling	+0.03 -0.03
Monte Carlo b/c efficiency	+0.03 -0.04
Monte Carlo $D^{*0} \varepsilon \cdot \text{Br}$	+0.02 -0.02
Monte Carlo statistics	+0.15 -0.15
$\text{Br}(D^0 \rightarrow K^- \pi^+)$	+0.06 -0.06
Total	± 0.22

Table 3: Summary of systematic uncertainties for the rate determined from the $D_{s1}^+ \rightarrow D^{*0}K^+$ channel.

reconstruction selects only D^0K^+ , such decays produce a cluster of events near a mass-difference of $700 \text{ MeV}/c^2$. This state has a natural width of $15 \text{ MeV}/c^2$. This, and the fact that the resolution is somewhat poorer at higher mass-differences, means that this contribution to the mass-difference distribution is much broader than that of the D_{s1}^+ . Based on the level of signal to background observed in the Monte Carlo analysis one does not expect that a contribution from this state would be observable above background in the analysis of the OPAL data.

The D^0K^+ mass-difference distribution obtained from the analysis of OPAL data is shown in figure 5(b). With the masses of the D_{s1}^+ and D^{*0} fixed to world average values [15] and the resolution fixed to the value obtained from Monte Carlo, the fit yields a signal of 28.7 ± 8.3 events. Parameterization of the signal as a single Gaussian, with both the mass and width allowed to vary, yielded a mass-difference of $527.3 \pm 2.2 \text{ MeV}/c^2$ and a width of $5.6 \pm 2.2 \text{ MeV}/c^2$, consistent with expectations.

Using the efficiency described above and accounting for the $D^0 \rightarrow K^- \pi^+$ branching ratio[15], the 28.7 ± 8.3 events observed correspond to a mean multiplicity, per hadronic Z^0 decay of

$$\bar{n}_{Z^0 \rightarrow D_{s1}^+ (x_E > 0.6)} \cdot \text{Br}(D_{s1}^+ \rightarrow D^{*0}K^+) = (1.9 \pm 0.5 \pm 0.2) \times 10^{-3}. \quad (27)$$

The quoted systematic uncertainty was determined by varying the choice of signal and background parameterizations, accounting for Monte Carlo statistics, the uncertainty on the D^0 and D^{*0} branching fractions and the uncertainty in the fraction of D_{s1}^+ candidates from $b\bar{b}$ and $c\bar{c}$ events. These contributions are discussed below and summarized in table 3.

The fit to the Monte Carlo distribution was found to reproduce the number of D_{s1}^+ decays, indicating that the background shape had been described adequately. Nevertheless, the effects of different background functions were considered as potential sources of systematic uncertainty. The other background parameterizations used were the Weibull function, $b(x) \propto ((x - m_K)/B)^{C-1} \exp(-((x - m_K)/B)^C)$, a second-order polynomial multiplied by a square-root threshold function, and a flat background above $0.51 \text{ GeV}/c^2$, with no threshold description.

Contributions due to the signal parameterization were also investigated. Possible effects due to an improperly determined mass resolution were estimated by varying the resolution, obtained from Monte Carlo, by $\pm 25\%$. The fit was also repeated with the signal parameterized by a Gaussian with the mass and width left free to vary.

Systematic uncertainties on the reconstruction efficiency arising from improperly modelled tracking resolution were estimated with Monte Carlo by redetermining the efficiencies with the resolutions of the track angles and impact parameters changed by $\pm 10\%$.

The use of asymmetric kaon dE/dx cuts can introduce systematic effects if the dE/dx is improperly modelled in the Monte Carlo. Such effects were studied using high-statistics samples of $D^{*+} \rightarrow (K^- \pi^+) \pi^+$ decays in both the data and Monte Carlo. Using the D^0 selection described above the relative efficiencies for the charged kaons to pass the dE/dx requirements were obtained. Good agreement was observed between data and Monte Carlo. The statistical uncertainty on this relative efficiency was used to assign a contribution to the systematic error.

In the accepted region of $x_E(D_{s1}^+) > 0.6$ there is a small residual contribution from D_{s1}^+ mesons produced in $b\bar{b}$ events. The systematic uncertainty associated with slightly different reconstruction efficiencies for D^{*0} mesons from $b\bar{b}$ and $c\bar{c}$ events was estimated by varying the b-contribution by $\pm 50\%$.

Finally, D_{s1}^+ decay sequences which proceed via $D^{*0} \rightarrow D^0 \gamma$ and $D^{*0} \rightarrow D^0 \pi^0$ also have slightly different reconstruction efficiencies. The systematic uncertainty attributable to this effect was estimated by folding the small efficiency difference together with the uncertainties on the D^{*0} branching fractions. The remaining contributions are from the uncertainty on the reconstruction efficiency due to limited Monte Carlo statistics, and from the uncertainty on the $D^0 \rightarrow K^- \pi^+$ branching ratio[15].

The stability of this measurement was checked by varying the cuts used to select the $D^{*0} K^+$ combinations. The following cuts were modified:

- The minimum x_{D^0} requirement was varied from 0.40 to 0.55.
- The minimum K^+ momentum was varied from 4.0 to 6.5 GeV/c.
- The minimum K^- and π^+ momenta were varied from 5.0 to 8.0 GeV/c.
- dE/dx weights for kaon identification were varied from ± 0.05 to ± 0.15 .
- The minimum D^0 decay length significance was varied from 0 to 1.

The changes in the measured rate introduced by variations of the selection criteria were consistent with the expected size of statistical fluctuations. Since there was no evidence for systematic effects not already accounted for, no additional systematic errors were assigned.

4.2 Analysis of the $D^{*+}K^0$ final state

The full decay chain used for the analysis of this channel was

$$\begin{array}{rcl}
 D_{s1}^+(2536) & \longrightarrow & D^{*+}K_S^0 \\
 & & \searrow \\
 & & D^0\pi^+ \\
 & & \searrow \\
 & & K^-\pi^+
 \end{array} \tag{28}$$

with D^{*+} candidates reconstructed using the selection described for the D^{**0} analysis in section 3. For this analysis, selected D^{*+} candidates were required to have a mass-difference in the range $143 < \Delta M(D^0\pi^+) < 148 \text{ MeV}/c^2$ in order to improve the signal to background ratio. Accepted D^{*+} candidates were combined with K_S^0 mesons reconstructed through their decays to $\pi^+\pi^-$, where the characteristic displaced vertex allows one to obtain a clean sample. For this decay channel it was essential to maintain a high reconstruction efficiency. For this reason, the cuts used to select $K_S^0 \rightarrow \pi^+\pi^-$ decays were relaxed from those used in other OPAL analyses [35]. The point of intersection of the π^+ and π^- was required to have a radial separation from the interaction point, R_{int} , in the range $1 < R_{\text{int}} < 150 \text{ cm}$. The angle between the vector joining the primary vertex to the point of intersection and the summed momentum vector of the π candidate tracks, computed at this point, was required to be less than 2 degrees. Good determination of the K_S^0 momentum was ensured by requiring that each track have either a minimum number of hits in the z -chambers, or that its endpoint be constrained to the z -coordinate of the end of the sensitive region of a jet chamber wire near the end-plate. No requirements were imposed on the transverse impact parameters of the tracks with respect to the primary vertex and only loose restrictions were imposed on the track separation in z at the point of intersection in the $r\phi$ plane. The invariant mass of the $\pi^+\pi^-$ pair was required to be in the range $0.45 < M(\pi^+\pi^-) < 0.54 \text{ GeV}/c^2$, which is wide compared with the intrinsic K_S^0 mass resolution. This reduces the systematic uncertainties associated with tails in the mass distribution.

Accepted $D^{*+}K_S^0$ combinations were required to satisfy $x_E > 0.6$. In this energy region, the efficiency for reconstructing the $D_{s1}^+ \rightarrow D^{*+}K_S^0$ decay was determined to be $(10.6 \pm 1.0)\%$ using Monte Carlo. Monte Carlo studies also showed that an improved mass-difference resolution could be obtained by considering the mass-difference calculated using

$$\Delta M(D^{*+}K_S^0) = M(D^{*+}K_S^0) - M(D^{*+}) - M(K_S^0) + M_{K_S^0}^{\text{nominal}} \tag{29}$$

where the nominal K_S^0 mass [15] was added to reproduce the usual mass-difference scale. For the $D^{*+}K_S^0$ selection just described, this yielded a resolution of $3.7 \pm 0.4 \text{ MeV}/c^2$.

The mass-difference distribution obtained from the OPAL hadronic Monte Carlo sample is shown in figure 6(a). Overlaid as a hatched distribution is the contribution from true $D_{s1}^+ \rightarrow D^{*+}K_S^0$ decays. The Monte Carlo distribution indicates that a signal from $D_{s1}^+ \rightarrow D^{*+}K_S^0$ decays should be seen near threshold. Although the Monte Carlo included the decay mode $D_{s2}^{*+} \rightarrow D^{*+}K_S^0$, this channel is phase-space suppressed relative to the DK final state. No $D_{s2}^{*+} \rightarrow D^{*+}K_S^0$ decays were reconstructed in the Monte Carlo sample.

Overlaid as a solid line is the result of an unbinned likelihood fit to the distribution. In this fit, the D_{s1}^+ signal was parameterized as a Gaussian with mass-difference fixed to the expected value[15] and width fixed to the resolution obtained from Monte Carlo studies. The background was parameterized by $b(x) \propto e^{-B(x-m_{K^0})}(x-m_{K^0})^C$ where m_{K^0} is the K^0 mass and B and C are free parameters. The fitted number of events in the Monte Carlo sample was $6.0_{-2.3}^{+2.8}$, consistent with the true value of 7.

The mass-difference distribution obtained from analysis of the OPAL data sample is shown in figure 6(b). Overlaid as a solid line is the result of a fit to the distribution with the same fit procedure described for the Monte Carlo analysis. However, because no events were observed at mass-differences below the signal, the threshold behaviour may not be adequately described by a freely varying background function. For this reason, the background was constrained to the shape determined from the fit to the distribution obtained from the Monte Carlo. Different background treatments were studied to estimate the systematic uncertainties. The fitted number of D_{s1}^+ decays observed in OPAL data was $N(D_{s1}^+) = 5.9_{-2.3}^{+2.8}$ which corresponds to a mean multiplicity per hadronic Z^0 decay of

$$\bar{n}_{Z^0 \rightarrow D_{s1}^+ (x_B > 0.6)} \cdot \text{Br}(D_{s1}^+ \rightarrow D^{*+} K^0) = (1.0_{-0.4}^{+0.5} \pm 0.1) \times 10^{-3}. \quad (30)$$

The contributions to the quoted systematic error are discussed below and summarized in table 4.

The systematic uncertainty associated with the background parameterization in the likelihood fit was estimated by refitting the mass-difference distribution with the unconstrained background function and with a polynomial multiplied by a square root threshold factor.

Effects associated with the signal parameterization were investigated by varying the mass-difference resolution by $\pm 25\%$. The corresponding systematic error was found to be negligible.

Systematic uncertainties on the reconstruction efficiency arising due to improperly modelled tracking resolution were estimated with Monte Carlo by redetermining the efficiencies with the impact parameter and angle resolutions changed by $\pm 10\%$.

The uncertainty resulting from different efficiencies for reconstructing D_{s1}^+ decays in $b\bar{b}$ and $c\bar{c}$ events was determined by varying the $b\bar{b}$ fraction by $\pm 50\%$ and was found to be negligible. The remaining uncertainties are due to finite Monte Carlo statistics and uncertainties on the D^{*+} and D^0 branching ratios.

The stability of this measurement was checked by varying the cuts used to select the $D^{*+} K_S^0$ combinations. The following cuts were modified:

- The width of the mass-difference window used to select D^{*+} candidates was varied between 4 and 6 MeV/c².
- The width of the $\pi^+ \pi^-$ mass window used to select K_S^0 candidates was varied between 50 and 130 MeV/c².
- The requirement that the K_S^0 tracks have hits in the z -chambers or the jet-chamber end-plate was removed.

Source	Uncertainty $\times 10^{-3}$
Background parameterization	+0.05 -0.02
Signal parameterization	< +0.005 -0.005
Tracking resolution	+0.03 -0.02
Monte Carlo b/c efficiency	< +0.005 -0.005
Monte Carlo statistics	+0.09 -0.09
$\text{Br}(D^{*+} \rightarrow D^0\pi^+) \cdot \text{Br}(D^0 \rightarrow K^-\pi^+)$	+0.04 -0.04
Total	+0.11 -0.10

Table 4: Summary of systematic uncertainties for the rate determined from the $D_{s1}^+ \rightarrow D^{*+}K_S^0$ channel.

The changes in the measured rate introduced by variations of the selection criteria were consistent with the expected size of statistical fluctuations. Since there was no evidence for systematic effects not already accounted for, no additional systematic errors were assigned.

Since the two rates, (27) and (30), are measured for the same region of $x_E(D_{s1}^+)$, taking the ratio of the two results yields a measurement of the ratio of branching ratios:

$$R \equiv \frac{\text{Br}(D_{s1}^+ \rightarrow D^{*0}K^+)}{\text{Br}(D_{s1}^+ \rightarrow D^{*+}K^0)} = 1.9^{+1.1}_{-0.9} \pm 0.4. \quad (31)$$

This is consistent with previous measurements [5, 7] and with the theoretical expectation discussed in section 4.

4.3 Calculation of $f(c \rightarrow D_{s1}^+(2536))$

Assuming that the decay width of the D_{s1}^+ is saturated by the D^*K final states, the mean multiplicity for the production of this state in hadronic Z^0 decays, for $x_E > 0.6$, is the sum of the two measured values shown in (27) and (30):

$$\bar{n}_{Z^0 \rightarrow D_{s1}^+(x_E > 0.6)} = \left(2.9^{+0.7}_{-0.6} \pm 0.2\right) \times 10^{-3}. \quad (32)$$

As stated in section 4.1, Monte Carlo studies indicated that the D_{s1}^+ signal with $x_E > 0.6$ has a small contribution from $b\bar{b}$ events. The expected contributions are about four events in the $D^{*0}K^+$ channel and one event in the $D^{*+}K_S^0$ analysis. Because of their inherent model dependence, these numbers were allowed to vary by $\pm 50\%$ when making the corresponding subtraction. Assuming the production of this state in charm fragmentation to be well modelled, one can then use Monte Carlo to extrapolate the result to the entire x_E range. The systematic error associated with this procedure was estimated by varying ϵ_c over a range of values consistent with OPAL measurements [28] of the mean x_E of D^0 and D^+ mesons produced in charm fragmentation. This was done in the manner described in section 3.4 for the D^{*0} analysis. Performing this extrapolation and writing the corrected rate in terms of the charm

hadronization factor, $f(c \rightarrow D_{s1}^+)$, defined as the fraction of charm quarks producing a D_{s1}^+ state in fragmentation, we obtain

$$2 \cdot \frac{\Gamma_{c\bar{c}}}{\Gamma_{\text{had}}} \cdot f(c \rightarrow D_{s1}^+(2536)) = (5.6 \pm_{-1.3}^{+1.5} \pm 0.6 \pm 0.8) \times 10^{-3} \quad (33)$$

where the second systematic error accounts for the combined uncertainties of the correction for the b-contribution and the extrapolation to the full range of x_E . The latter contribution includes the uncertainty arising from the use of different fragmentation models[33]. Using $\Gamma_{c\bar{c}}/\Gamma_{\text{had}} = 0.172$ [34] this corresponds to the branching fraction

$$f(c \rightarrow D_{s1}^+) = 0.016 \pm 0.004 \pm 0.003. \quad (34)$$

5 Discussion

The measured D^{*0} production rates in charm quark fragmentation can be compared with predictions made using simplified assumptions about fragmentation. Based on fits to the production rates of light-flavoured hadrons, predictions have been made for the average production rates of heavy flavoured hadrons [36]. These include $f(c \rightarrow (D_1 + D_2)_{u,d}) = 0.170$ and $f(c \rightarrow D_{s1} + D_{s2}^*) = 0.028$. Assuming isospin symmetry, the former implies $f(c \rightarrow D^{*0}) = 0.085$ which agrees well with the measured rate shown in equation (20). The ratio $f(c \rightarrow D_1^0)/f(c \rightarrow D_2^{*0})$ is calculated from the measured value of $f_1^{c\bar{c}}$ yielding

$$\frac{f(c \rightarrow D_1^0)}{f(c \rightarrow D_2^{*0})} = 0.40 \pm 0.25 \pm 0.10, \quad (35)$$

where correlations in the systematic uncertainties have been taken into account. This value is consistent with the simple spin-counting prediction of 3/5.

A prediction for the combined rate of D_{s1}^+ and D_{s2}^{*+} production was presented in [36]. The approximate degeneracy in the D_{s1}^+ and D_{s2}^{*+} masses allows predictions for the individual production rates to be estimated using spin-counting arguments in the context of this model. This results in the prediction $f(c \rightarrow D_{s1}^+) = 0.011$ which is consistent with the measurement given in equation (34). This is a test of strange-quark suppression.

OPAL has also observed the production of P-wave B mesons in hadronic Z^0 decays [16] and has measured the relative branching fractions:

$$\frac{\Gamma(Z^0 \rightarrow \bar{b} \rightarrow B^{*0} \rightarrow B^{(*)+}\pi^-)}{\Gamma(Z^0 \rightarrow \bar{b} \rightarrow B^+)} = 0.18 \pm 0.04 \quad (36)$$

and

$$\frac{\Gamma(Z^0 \rightarrow \bar{b} \rightarrow B_s^{*0} \rightarrow B^{(*)+}K^-)}{\Gamma(Z^0 \rightarrow \bar{b} \rightarrow B^+)} = 0.026 \pm 0.008. \quad (37)$$

Measurements of the former quantity have also been published by the DELPHI[17] and ALEPH[18] collaborations, in each case yielding results consistent with the OPAL measurement.

Assuming that the B_{s1}^0 and B_{s2}^{*0} states are produced in a ratio of 3/5 (from spin-statistics), that $\text{Br}(B_s^{**0} \rightarrow B^{(*)+}K^-) = 1/2$ and $\text{Br}(B_s^{**0} \rightarrow B^{(*)+}\pi^-) = 2/3$ (from isospin invariance), and that B^0 and B^+ mesons are produced at equal rates in b-quark fragmentation, then using $f(\bar{b} \rightarrow B^+) = 0.378 \pm 0.022$ [15], we obtain

$$f(\bar{b} \rightarrow B_s^{**0}) = 0.10 \pm 0.02 \quad (38)$$

and

$$f(\bar{b} \rightarrow B_{s1}^0) = 0.007 \pm 0.002. \quad (39)$$

These value are similar to the corresponding fractions for the production of excited charm and charm-strange mesons in charm fragmentation.

Measurements of P-wave meson production in the light-quark sector have been performed by OPAL[37] and DELPHI[38]. However, since the relative mass-differences between the P-wave states and the corresponding pseudoscalar and vector ground-state mesons are much larger in the light-quark sector than for B or D mesons, it is difficult to draw conclusions from direct comparisons of the relative production rates.

6 Conclusions

We have measured the mean multiplicities for production of $D_1^0(2420)$ and $D_2^{*0}(2460)$ mesons in Z^0 decays. The measured values are

$$\bar{n}_{Z^0 \rightarrow c\bar{c} \rightarrow D^{**0}(x_E > 0.5)} \cdot \text{Br}(D^{**0} \rightarrow D^{*+}\pi^-) = \left(5.4 \begin{smallmatrix} +1.4 & +0.6 \\ -1.3 & -0.8 \end{smallmatrix}\right) \times 10^{-3} \quad (40)$$

$$\bar{n}_{Z^0 \rightarrow b\bar{b} \rightarrow D^{**0}(x_E > 0.2)} \cdot \text{Br}(D^{**0} \rightarrow D^{*+}\pi^-) = \left(16.1 \begin{smallmatrix} +3.7 & +2.0 \\ -3.6 & -1.8 \end{smallmatrix}\right) \times 10^{-3} \quad (41)$$

The fraction of the D^{**0} signal due to the D_1^0 state was determined to be

$$f_1^{c\bar{c}} = 0.56 \pm 0.15 \begin{smallmatrix} +0.03 \\ -0.04 \end{smallmatrix} \quad (42)$$

and

$$f_1^{b\bar{b}} = 0.77 \begin{smallmatrix} +0.16 \\ -0.14 \end{smallmatrix} \pm 0.04, \quad (43)$$

for D^{**0} production in $c\bar{c}$ and $b\bar{b}$ events, respectively.

Extrapolating the mean multiplicity measurements in $c\bar{c}$ events to the full region of $x_E(D^{**0})$ and using the the quoted value of $f_1^{c\bar{c}}$, we estimate the fractions of charm quarks producing these states in fragmentation to be

$$f(c \rightarrow D_1^0) = 0.021 \pm 0.007 \pm 0.003 \quad (44)$$

and

$$f(c \rightarrow D_2^{*0}) = 0.052 \pm 0.022 \pm 0.013 \quad (45)$$

where the systematic uncertainty includes the model dependence introduced by the extrapolation of the measured rates to the full range of x_E . The combination of these results yields

$$f(c \rightarrow D^{*0}) = 0.073 \pm 0.023 \pm 0.014. \quad (46)$$

The corresponding fractions of b-hadron decays producing these states are

$$f(b \rightarrow D_1^0) = 0.050 \pm 0.014 \pm 0.006, \quad (47)$$

$$f(b \rightarrow D_2^{*0}) = 0.047 \pm 0.024 \pm 0.013, \quad (48)$$

and

$$f(b \rightarrow D^{*0}) = 0.097 \pm 0.035 \pm 0.017. \quad (49)$$

The $D_{s1}^+(2536)$ meson has been observed in both the $D^{*0}K^+$ and $D^{*+}K_s^0$ final states. The measured mean multiplicity for production of this state in hadronic Z^0 decays is

$$\bar{n}_{Z^0 \rightarrow D_{s1}^+(x_E > 0.6)} = \left(2.9 \begin{smallmatrix} +0.7 \\ -0.6 \end{smallmatrix} \pm 0.2 \right) \times 10^{-3} \quad (50)$$

for the quoted region of x_E . The ratio of branching ratios for the two final states is

$$R \equiv \frac{\text{Br}(D_{s1}^+ \rightarrow D^{*0}K^+)}{\text{Br}(D_{s1}^+ \rightarrow D^{*+}K^0)} = 1.9 \begin{smallmatrix} +1.1 \\ -0.9 \end{smallmatrix} \pm 0.4. \quad (51)$$

Using Monte Carlo to correct for small contributions from $b\bar{b}$ events and for extrapolation of the mean-multiplicity measurement to the full region of x_E , we obtain an estimate for the fraction of charm quarks producing D_{s1}^+ mesons:

$$f(c \rightarrow D_{s1}^+) = 0.016 \pm 0.004 \pm 0.003. \quad (52)$$

All production fractions are found to be similar in magnitude to the corresponding production fractions in the b-quark sector. The results obtained in this analysis are consistent with predictions based on current understanding of the heavy-quark fragmentation process.

Acknowledgements

We particularly wish to thank the SL Division for the efficient operation of the LEP accelerator and for their continuing close cooperation with our experimental group. We thank our colleagues from CEA, DAPNIA/SPP, CE-Saclay for their efforts over the years on the time-of-flight and trigger systems which we continue to use. In addition to the support staff at our own institutions we are pleased to acknowledge the
Department of Energy, USA,
National Science Foundation, USA,
Particle Physics and Astronomy Research Council, UK,
Natural Sciences and Engineering Research Council, Canada,
Israel Science Foundation, administered by the Israel Academy of Science and Humanities,
Minerva Gesellschaft,
Benozio Center for High Energy Physics,
Japanese Ministry of Education, Science and Culture (the Monbusho) and a grant under the Monbusho International Science Research Program,
German Israeli Bi-national Science Foundation (GIF),
Direction des Sciences de la Matière du Commissariat à l'Énergie Atomique, France,
Bundesministerium für Bildung, Wissenschaft, Forschung und Technologie, Germany,
National Research Council of Canada,
Hungarian Foundation for Scientific Research, OTKA T-016660, T023793 and OTKA F-023259.

References

- [1] N. Isgur and M. B. Wise, *Phys. Rev. Lett.* **66** (1991) 1130.
- [2] J. L. Rosner, *Comments Nucl. Part. Phys.* **16** (1986) 109.
- [3] ARGUS Collaboration, H. Albrecht, *et al.*, *Phys. Rev. Lett.* **56** (1986) 549, *Phys. Lett.* **B221** (1989) 422, *Phys. Lett.* **B231** (1989) 208, *Z. Phys.* **C69** (1996) 405.
- [4] ARGUS Collaboration, H. Albrecht, *et al.*, *Phys. Lett.* **B232** (1989) 398.
- [5] ARGUS Collaboration, H. Albrecht, *et al.*, *Phys. Lett.* **B230** (1989) 162.
- [6] ARGUS Collaboration, H. Albrecht, *et al.*, *Phys. Lett.* **B297** (1992) 425.
- [7] CLEO Collaboration, P. Avery, *et al.*, *Phys. Rev.* **D41** (1990) 774, *Phys. Lett.* **B303** (1993) 377, *Phys. Lett.* **B340** (1994) 194.
- [8] CLEO Collaboration, P. Avery, *et al.*, *Phys. Lett.* **B331** (1994) 236.
- [9] CLEO Collaboration, Y. Kubota, *et al.*, *Phys. Rev. Lett.* **72** (1994) 1972.
- [10] E691 Collaboration, J.C. Anjos, *et al.*, *Phys. Rev. Lett.* **62** (1989) 1717.

- [11] E687 Collaboration, P.L. Frabetti, *et al.*, Phys. Rev. Lett. **72** (1994) 324.
- [12] BEBC Collaboration, A.E. Asratian, *et al.*, Z. Phys. **C61** (1994) 563.
- [13] OPAL Collaboration, R. Akers, *et al.*, Z. Phys. **C67** (1995) 57.
- [14] ALEPH Collaboration, D. Buskulic, *et al.*, Phys. Lett. **B345** (1994) 103,
Z. Phys. **C62** (1994) 1, Z. Phys. **C73** (1997) 601.
- [15] Particle Data Group, R.M. Barnett, *et al.*, Phys. Rev. **D54** (1996) 1.
- [16] OPAL Collaboration, R. Akers, *et al.*, Z. Phys. **C66** (1995) 19.
- [17] DELPHI Collaboration, P. Abreu, *et al.*, Phys. Lett. **B345** (1995) 598.
- [18] ALEPH Collaboration, D. Abbaneo, *et al.*, Z. Phys. **C69** (1996) 393.
- [19] OPAL Collaboration, K. Ahmet *et al.*, Nucl. Instrum. Methods **A305** (1991) 275.
- [20] P.P. Allport, *et al.*, Nucl. Instrum. Methods **A324** (1993) 34.
- [21] P.P. Allport, *et al.*, Nucl. Instrum. Methods **A346** (1994) 476.
- [22] OPAL Collaboration, G. Alexander *et al.*, Z. Phys. **C52** (1991) 175.
- [23] T. Sjöstrand, Comp. Phys. Comm. **39** (1986) 347;
T. Sjöstrand and M. Bengtsson, Comp. Phys. Comm. **43** (1987) 367;
T. Sjöstrand, CERN-TH 6488/92.
- [24] T. Sjöstrand, JETSET 7.4 Manual, CERN-TH 7112/93.
- [25] J. Allison, *et al.*, Nucl. Instrum. Methods **A317** (1992) 47.
- [26] C. Peterson, *et al.*, Phys. Rev. **D27** (1983) 105.
- [27] OPAL Collaboration, G. Alexander, *et al.*, Phys. Lett. **B364** (1995) 93.
- [28] OPAL Collaboration, G. Alexander, *et al.*, Z. Phys. **C72** (1996) 1.
- [29] S. Godfrey and R. Kokoski, Phys Rev. **D43** (1991) 1679.
The quoted values have been recalculated using experimentally observed masses.
- [30] OPAL Collaboration, R. Akers, *et al.*, Z. Phys. **C67** (1995) 27.
- [31] CDF Collaboration, F. Abe *et al.*, Phys. Rev. **D45** (1992) 1448.
- [32] OPAL Collaboration, P.D. Acton, *et al.*, Phys. Lett. **B273** (1991) 355.
- [33] P. Collins and T. Spiller, J. Phys. **G11** (1985) 1289;
V.G. Kartvelishvili, A.K. Likhoded and V.A. Petrov, Phys. Lett. **B78** (1978) 615;
B. Andersson, G. Gustafson and B. Söderberg, Z. Phys. **C20** (1983) 317.

- [34] The current world average values[15] for R_c and R_b are consistent with Standard Model predictions. Accounting for the experimental uncertainties would introduce only a negligible contribution to the systematic error.
- [35] OPAL Collaboration, R. Akers, *et al.*, Z. Phys. **C67** (1995) 389.
- [36] Yi-Jin Pei, Z. Phys. **C72** (1996) 39.
- [37] OPAL Collaboration, R. Akers, *et al.*, Z. Phys. **C68** (1995) 1.
- [38] DELPHI Collaboration, P. Abreu, *et al.*, CERN-PPE/96-77, Submitted to Z. Physik **C**, Phys. Lett. **B379** (1996) 309, Z. Phys. **C65** (1995) 587.

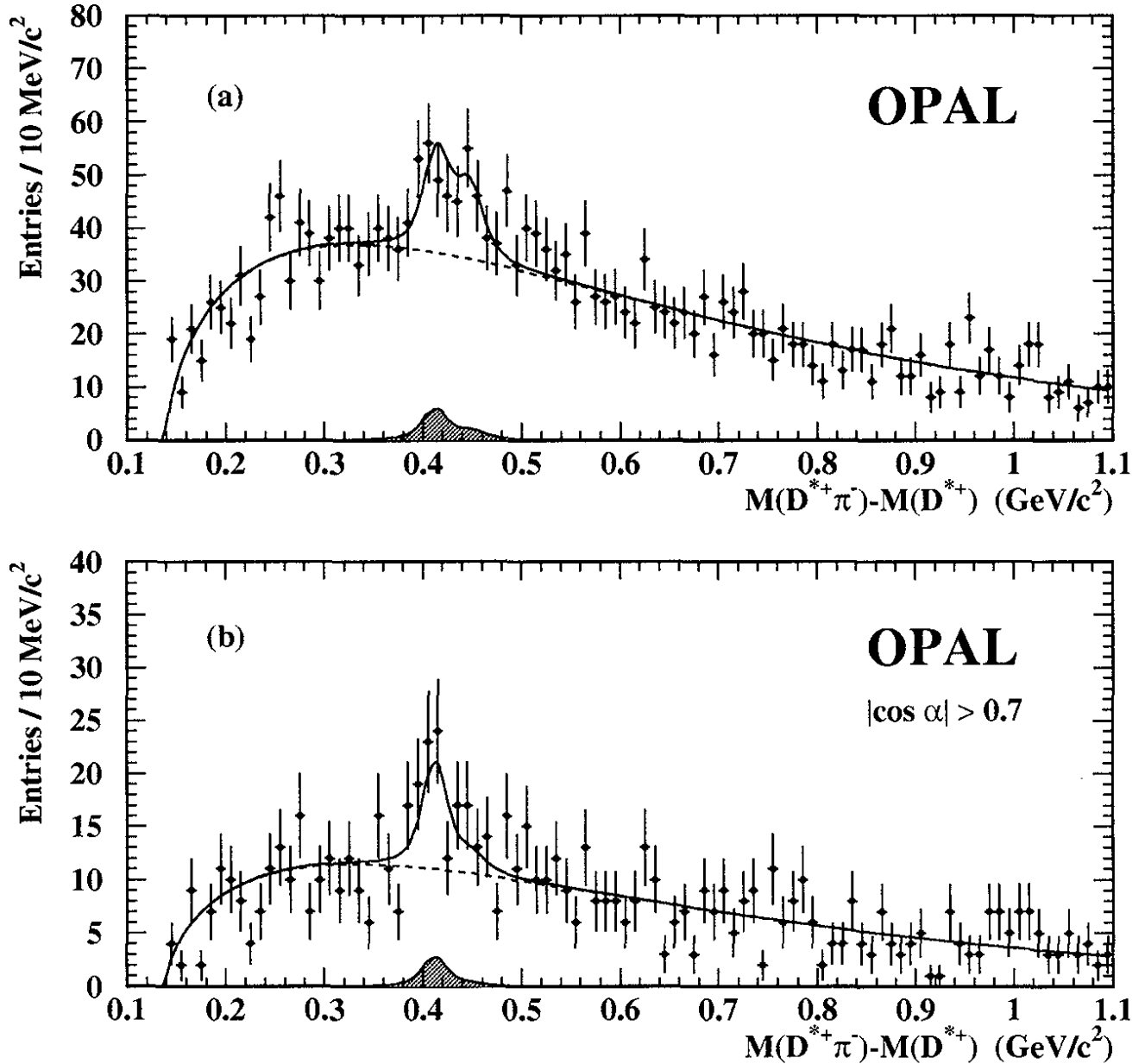


Figure 1: $M(D^{*+}\pi^-) - M(D^{*+})$ distribution for the charm-enriched sample with (a) no restriction on the helicity angle and (b) for $|\cos \alpha| > 0.7$. In each case, the shaded distribution shows the expected contribution from bottom flavoured events, determined from the simultaneous fit. Overlaid as a solid line is the fit result. The fit result shown in (b) is not the result of a separate fit but is obtained by integrating the likelihood function from the fit to the full distribution over the region $|\cos \alpha| > 0.7$. In each case, the dashed line indicates the background component of the fit result.

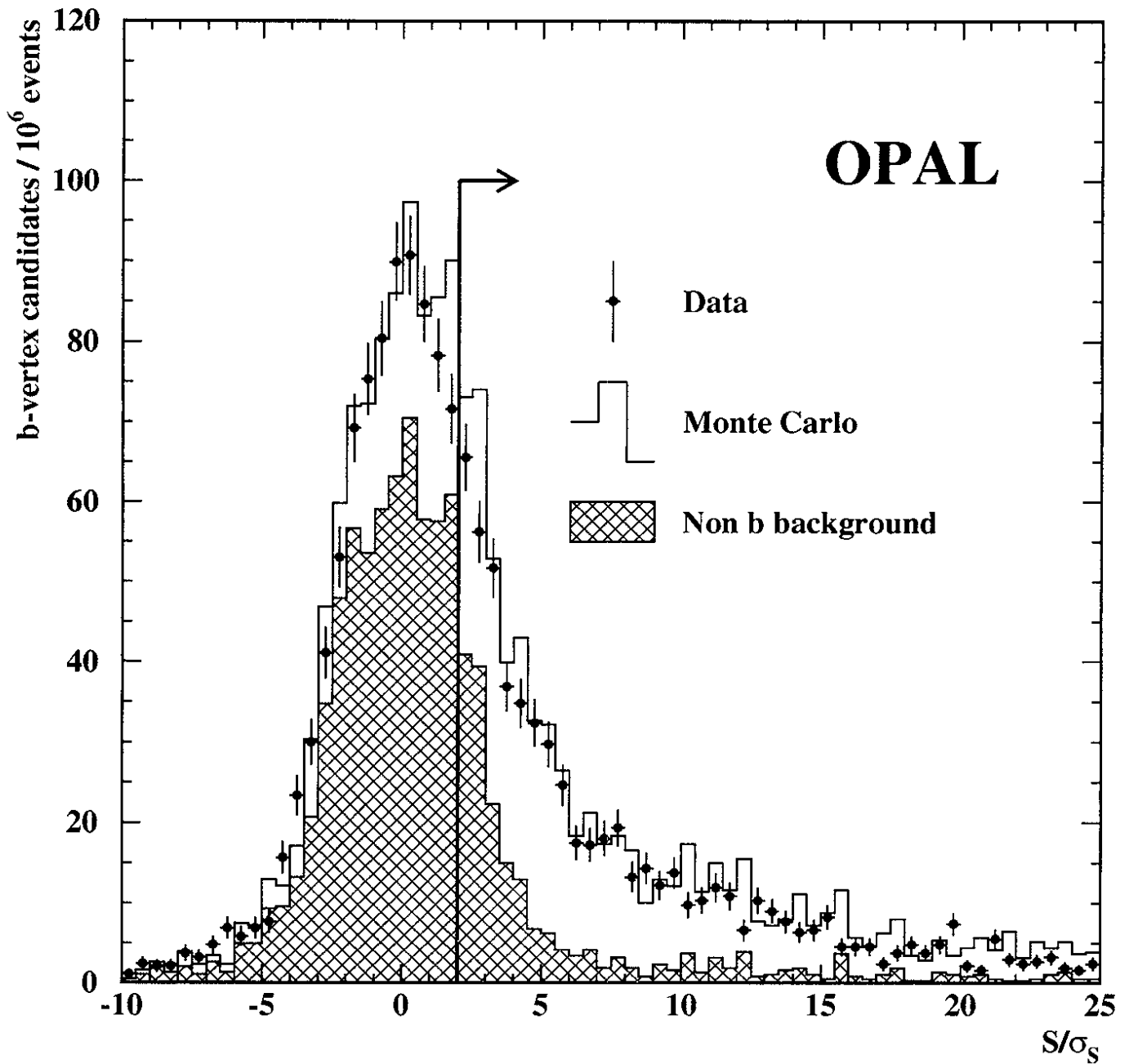


Figure 2: Decay length significance distribution for the b hadron from the $b \rightarrow D^{*+}X$ decay. The open histogram shows the distribution obtained from Monte Carlo. The points with error bars are from analysis of the OPAL data. The hatched histogram shows the expected contributions from charm and light flavour events, from Monte Carlo. The arrow indicates the cut of $S/\sigma_S > 2$ used in the selection.

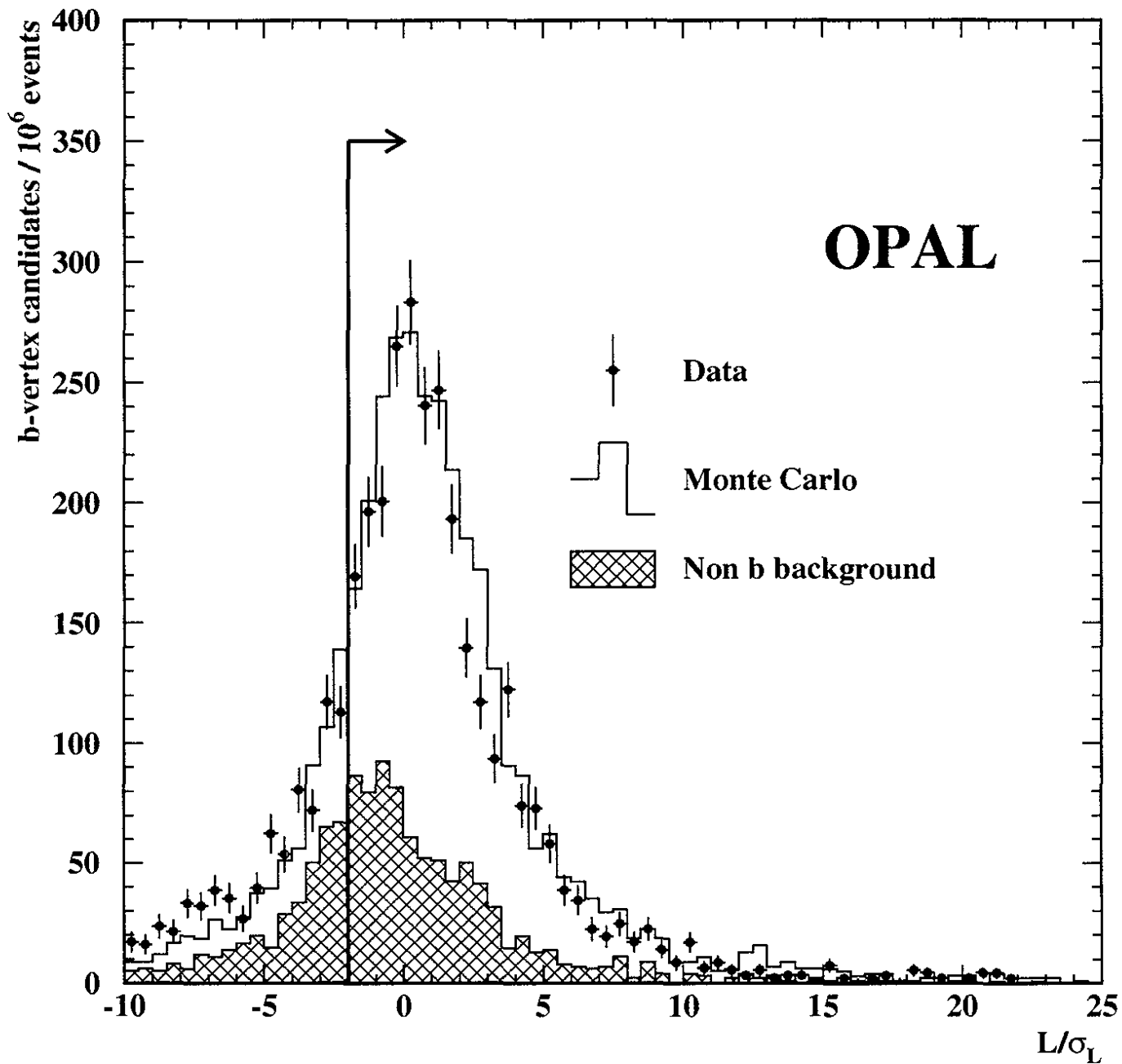


Figure 3: Decay length significance distribution for the D^0 from the $b \rightarrow D^{*+}X, D^{*+} \rightarrow D^0\pi^+$ decay sequence. The open histogram shows the distribution obtained from Monte Carlo. The points with error bars are from analysis of the OPAL data. The hatched histogram shows the expected population from charm and light flavour events and the arrow indicates the cut of $L/\sigma_L > -2$ requirement used in the selection.

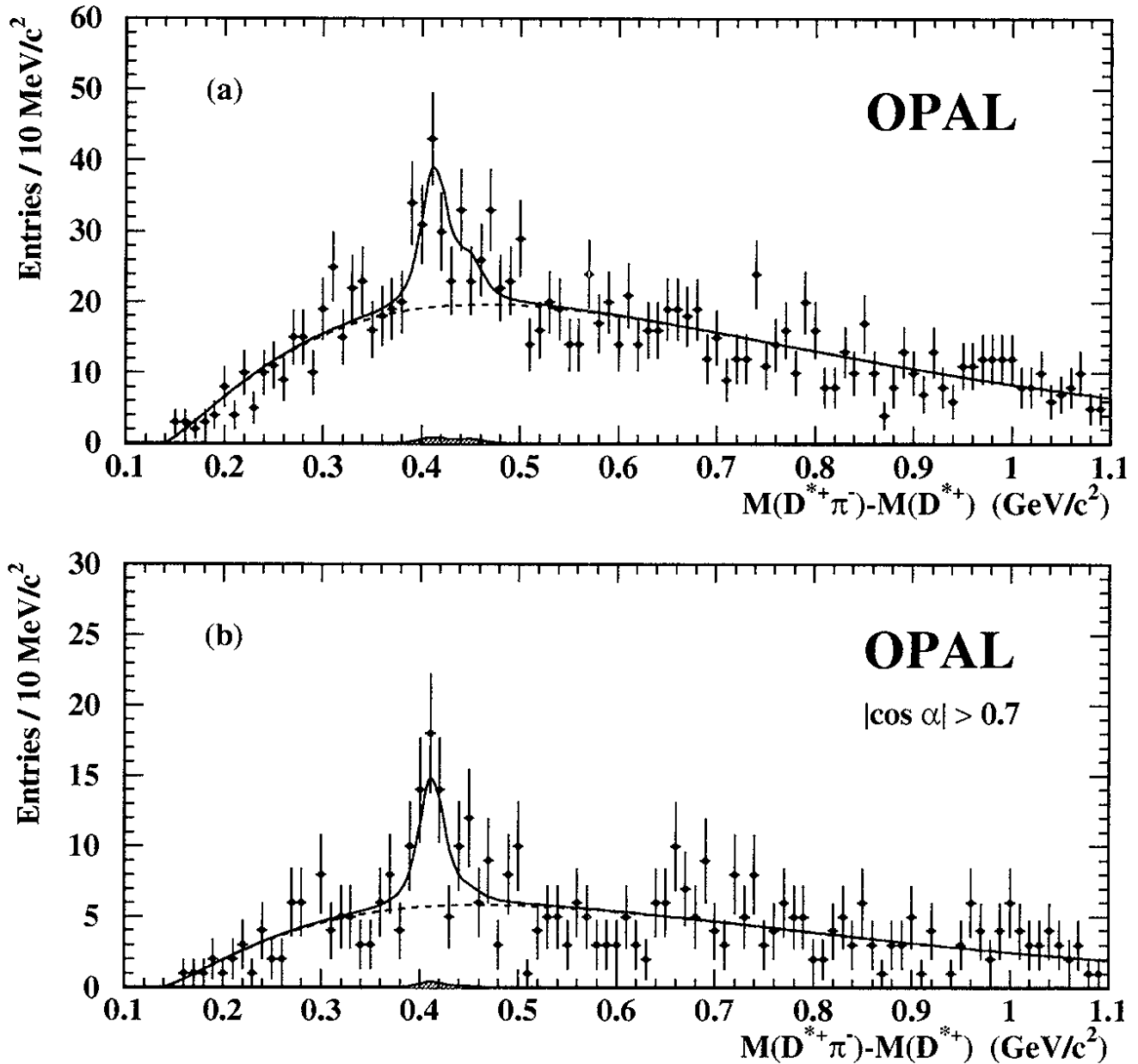


Figure 4: $M(D^{*+}\pi^-) - M(D^{*+})$ distribution for the bottom-enriched sample with (a) no restriction on the helicity angle and (b) for $|\cos \alpha| > 0.7$. In each case, the shaded histogram shows the expected contribution from charm fragmentation, determined from the simultaneous fit. Overlaid as a solid line is the fit result. The fit result shown in (b) is not the result of a separate fit but is obtained by integrating the likelihood function from the fit to the full distribution over the region $|\cos \alpha| > 0.7$. In each case, the dashed line indicates the background component of the fit result.

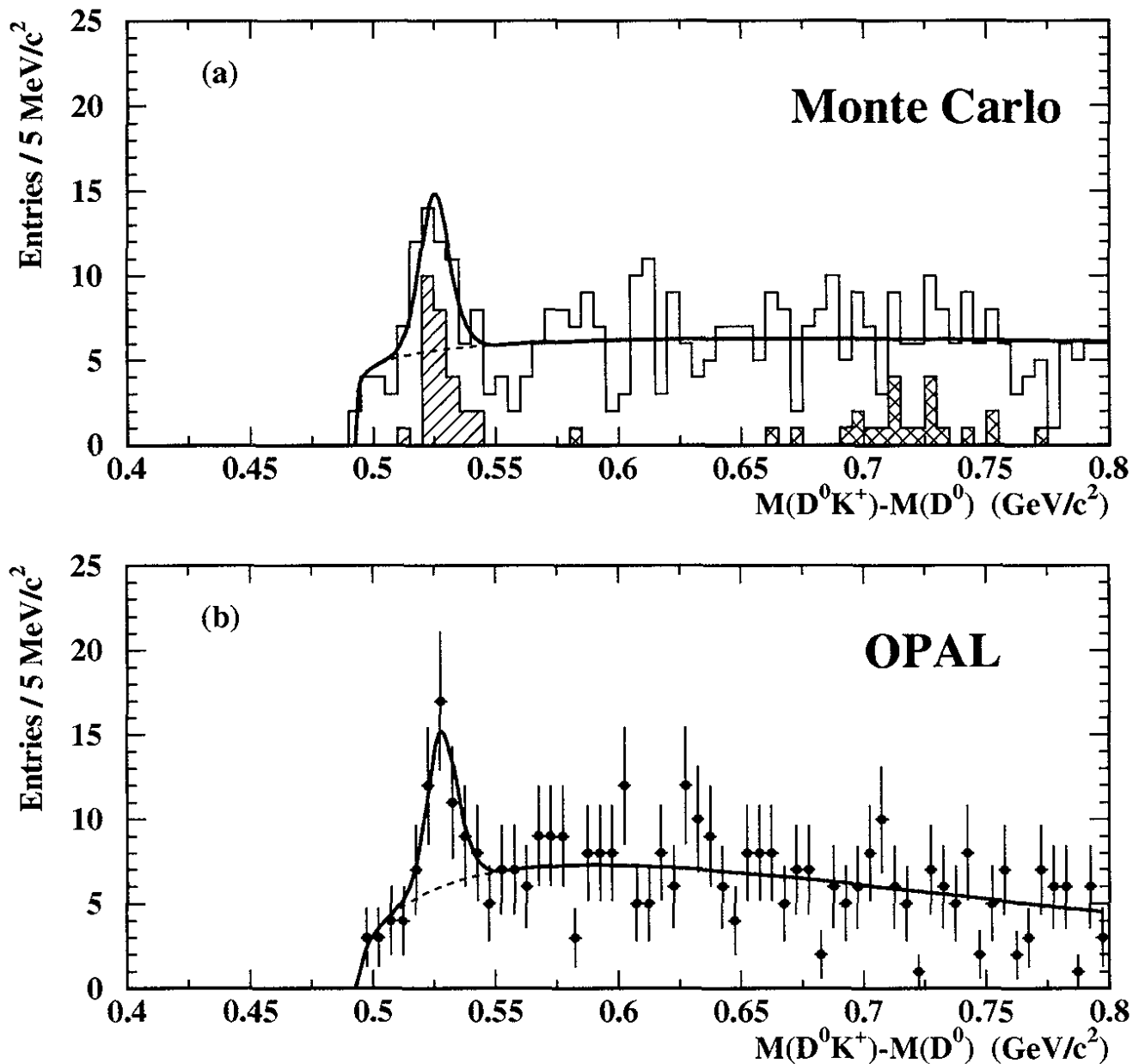


Figure 5: Mass-difference distributions in the $D^0 K^+$ channel from (a) OPAL Monte Carlo and (b) the OPAL hadronic data sample. The solid curves are the result of the fit described in the text, while the dashed curves show the fitted background component. In (a), the hatched distribution under the fitted peak indicates the contribution from $D_{s1}^+ \rightarrow D^{*0} K^+$ decays, while the cross-hatched distribution at higher mass-differences shows the contribution from $D_{s2}^{*+} \rightarrow D^0 K^+$.

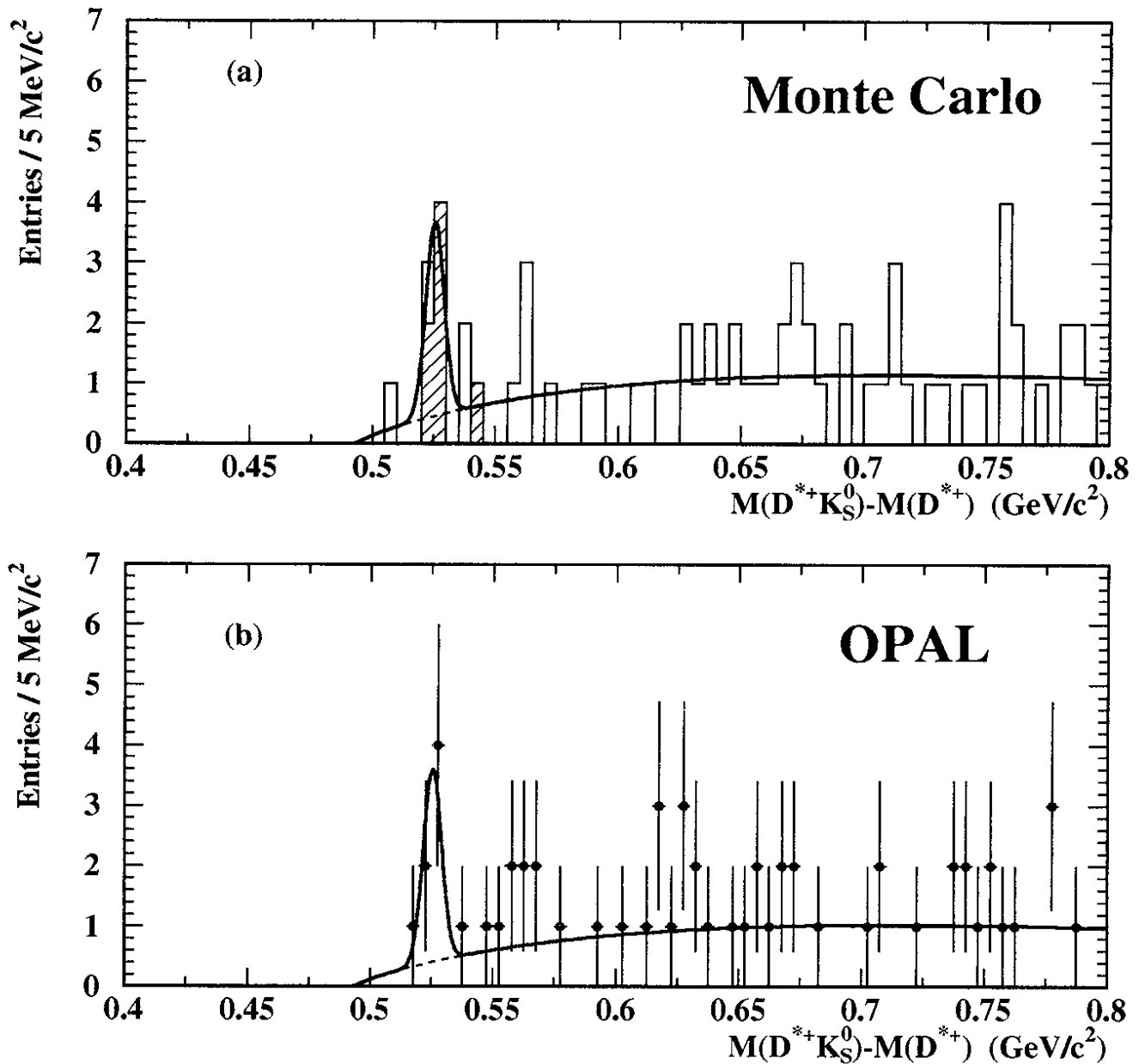


Figure 6: Mass-difference distributions in the $D^{*+}K_S^0$ channel from (a) OPAL Monte Carlo and (b) the OPAL hadronic data sample. The solid curves are the result of the fit described in the text, while the dashed curves show the fitted background component. The hatched distribution in (a) shows the contribution from D_{s1}^+ decays.